Mon. Not. R. astr. Soc. (1992) **254,** 30–50

A compilation of active and normal galaxies observed in both infrared and X-rays

Paul J. Green,[1] Scott F. Anderson[1] and Martin J. Ward[2]
[1] *Department of Astronomy, FM-20, University of Washington, Seattle, WA 98195, USA*
[2] *Department of Physics, Nuclear Physics Building, Keble Road, University of Oxford, Oxford OX1 3RH*

Accepted 1991 August 13. Received 1991 July 22; in original form 1991 May 1.

SUMMARY

For the largest ensemble of active and normal galaxies to date, we have collected far-infrared and X-ray data from the literature and from the *IRAS* and *Einstein* databases. We study the relation between emission in these two bands, using survival analysis to exploit the information contained in upper limits.

We find that galaxies with soft X-ray to infrared flux ratios greater than about 0.01 are almost certain to show broad-line optical emission. This discriminant will be valuable for finding quasars and Seyfert 1 galaxies from comparisons of IR and X-ray surveys. A sensitive, all-sky X-ray survey like *ROSAT* is particularly well-suited to such a search in conjunction with the *IRAS* data.

For the full *IRAS*/*Einstein* ensemble, we find a significant correlation between luminosities in the 60-μm and 0.5–4.5 keV bands. A strong offset separates broad-line from normal and narrow-line galaxies. We interpret the jump toward higher X-ray emission in broad-line galaxies as evidence for the increasing importance of a non-thermal nuclear source. Among individual galaxy classes, radio-loud quasars show a significant correlation of L_X to $L_{60\,\mu\mathrm{m}}$ that is not seen in radio-quiet quasars or Seyferts as individual classes. Since the ratios $L_X/L_{60\,\mu\mathrm{m}}$ differ significantly between predominantly thermal and non-thermal nuclear components, we conjecture that the correlations intrinsic to each individual component are lost when the two are strongly mixed in Seyfert galaxies or radio-quiet quasars.

Our analysis of the empirical relationship between L_X and $L_{60\,\mu\mathrm{m}}$ for normal and narrow optical emission-line galaxies (excluding Seyfert 2s) allows us to convert published 60-μm *IRAS* luminosity functions into estimates of the 2-keV X-ray luminosity function of IR-emitting galaxies. We use this luminosity function to estimate the contribution to the soft X-ray background of these lower luminosity IR-emitting galaxies out to $z_{\max}=3$. Depending on the evolutionary model applied, we derive contributions of 5–25 per cent for these galaxies to the soft X-ray background.

1 INTRODUCTION

Non-thermal continuum radiation from active galactic nuclei (AGN) can span many decades in energy, from the radio through the γ-ray region. The spectral energy distributions of AGN are modelled by several components. These include non-thermal synchrotron radiation, thermal radiation from an accretion disc, stars and H II regions, dust, or clouds of gas. Correlations between fluxes in disparate wavebands may contain important empirical clues to the physics of radiation emission mechanisms in the central source.

Correlations between near-infrared, optical and X-ray luminosities have been amply demonstrated in quasars and Seyferts (e.g. Dahari & DeRobertis 1988; Edelson, Malkan & Rieke 1987). The form and strength of the correlation may reveal information about the energetics and sources of emission. Lower ratios of X-ray to optical luminosity have been noted as quasars tend toward higher luminosity or redshift such that $L_X \propto L_{\mathrm{opt}}^{0.7}$ (Kriss & Canizares 1985; Tananbaum *et al.* 1986). A similarly non-linear dependence has also been found between near-infrared and X-ray radiation (Worrall 1987; Kriss 1988), but the primary dependences are unclear. Is some of the infrared radiation due to optical, UV, or possibly soft X-ray energy that has been absorbed and re-radiated at longer wavelengths? Or are the X-rays from inverse Compton scattering of infrared photons off

relativistic electrons? Recently, Done *et al.* (1990) showed that the latter is not the case for NGC 4051, since X-ray and infrared variability are not correlated. In some cases, characteristic power-law spectral slopes appear to persist between wavebands, but in other cases may disappear or possibly be contaminated by stellar and/or thermal radiation. Near-infrared emission in quasars may fit a power-law that extrapolates well to soft X-ray emission near 2 keV. The intervention of the UV 'big bump', peaking near 2500 Å, could be the result of thermal radiation from an accretion disc around a black hole (e.g. Malkan & Sargent 1982). Power-law-like spectra reappear in the X-ray continuum where, for quasars, spectral index is related to radio loudness (Wilkes & Elvis 1987), and so also to the strength of a central non-thermal synchrotron source.

Both active nuclei (powered by accretion on to a massive compact object) and the by-products of rapid star formation contribute to the X-ray radiation of active galaxies. X-ray radiation from regions of intense star formation (a starburst, Rieke *et al.* 1980; Fabbiano & Trinchieri 1984) are interpreted as arising from Population I objects (OB stars, supernovae, and massive X-ray binaries). The overwhelming source of X-ray emission in QSOs and Seyfert galaxies is the nucleus.

The source of infrared radiation in active galaxies is still controversial, but the most favoured *nuclear* emission mechanisms are thermal (from warm nuclear dust) and non-thermal (from synchrotron radiation). Non-thermal models of IR properties in AGN are based on the small percentage of (optically selected) quasars that have strong, flat-spectrum radio emission. Such objects also show rapid IR variability and high brightness temperatures, consistent with the current models of optically thin synchrotron emission from the inner radio jet. Emission from stars and cool dust in the AGN host galaxy may also contribute a substantial fraction of the IR radiation, particularly for the lower luminosity nuclei. The source which heats the nuclear dust is primarily the intense UV/optical continuum coming from the compact nucleus (Barvainis 1990).

The X-ray properties of the so-called normal galaxies have been extensively reviewed by Fabbiano (1989). In another paper with coworkers (Fabbiano, Gioia & Trinchieri 1988), she investigated correlations between the infrared and X-ray continuum from spiral galaxies, but the non-parametric tests then available disregarded X-ray upper limits. Some correlation of far-infrared with X-ray radiation is expected *a priori* in spiral and irregular galaxies, since their young star-formation regions produce Pop. I X-ray sources (OB stars, supernovae, and massive X-ray binaries) along with warm dust. For elliptical galaxies, several results have pointed to a hot interstellar medium as the predominant source of X-ray emission. Hot gas is thought to dominate the X-ray emission in elliptical galaxies of high luminosity ($L_X > 10^{41}$ erg s^{-1}), whereas X-rays in low-luminosity ellipticals can be entirely accounted for by Population II low-mass X-ray binaries.

Clearly, the physical models proposed are diverse and are often tailored to match observations in a narrow parameter space, or for a very select galaxy sample. Larger samples bringing together both active and normal galaxies can constrain the proliferation of models and permit sound statistical tests that complement more anecdotal results.

We have compiled, for a total of 269 quasars, Seyferts, emission-line and normal galaxies, infrared and X-ray data from the *IRAS* and *Einstein* satellites. We normalize the heterogeneous published X-ray data to a single bandpass, 0.5–4.5 keV. To minimize aperture effects and increase sensitivity, we adopt infrared data from *IRAS* pointed observations, coadded scans, and the Point Source Catalog (1985). Using non-parametric univariate tests, we contrast these data for all galaxy classes in our list. Bivariate correlations between variables are also tested, and we determine regressions for all variable pairs showing a significant correlation. To minimize selection effects, censored points (limits) are properly treated via survival analysis (Isobe, Feigelson & Nelson 1986).

In Section 2, the constituent galaxies of our data set and possible selection effects are discussed. In Section 3, we describe the data set, and our methods to maximize its consistency. This is followed in Section 4 by statistical results: first the univariate means and two-sample tests, and then results of bivariate (correlation and regression) analysis. Section 5 investigates the individual classes of galaxy. We use our data set in Section 6, combined with published infrared luminosity functions, to investigate the contribution of lower luminosity galaxies to the X-ray background. Our conclusions are presented in Section 7, with statistical methods detailed in the Appendix.

2 THE *IRAS/EINSTEIN* COMPILATION

The essential criterion for inclusion in our data set is that either detections or upper limits exist for a galaxy in both the *IRAS* Point Source Catalog (PSC) and *Einstein* databases. The only exception to this is for quasars, very few of which were detected in the PSC. For these we include data from pointed observations. Our full *IRAS/Einstein* (hereafter, IR/X) compilation spans a wide range of galaxy activity, from normal galaxies through quasars.

A more complete sample of galaxies could be obtained by coadding *IRAS* data for every AGN ever observed by *Einstein* either serendipitously or in a targeted observation. The *Einstein* Medium Sensitivity Survey (Gioia *et al.* 1990), now under way, will eventually yield an X-ray flux-limited sample of AGN discovered 'serendipitously' in IPC images. During its lifetime, the *Einstein Observatory* surveyed only about 4 per cent of the sky, targeting almost exclusively objects previously observed in other (usually optical or radio) frequency bands. Although the energy range will be softer than that of *Einstein*, the *ROSAT* all-sky survey will eventually provide a more homogeneous X-ray data set. A comparison study of *IRAS* coadded data for galaxies in these surveys will yield statistics largely uninfluenced by the diverse optical and radio selection effects present when studying galaxies that are *Einstein* targets. Such a project, however, is still years from completion.

A much smaller study has already been performed (Green *et al.* 1989, hereafter Paper I), using only serendipitous *Einstein* observations of 'warm' *IRAS* galaxies [$\alpha(25, 60) \geq -1.5$]. The resulting *IRAS*-selected sample suffers from neither X-ray nor optical selection effects. These 16 warm *IRAS* galaxies have been included in the present study.

The seven sub-classes of galaxy that we have adopted for analysis (followed here by their abbreviations) follow standard classifications based on optical properties: quasar (QSO), Seyfert 1 (Sy1), Seyfert 2 (Sy2), starburst or giant extragalactic H II emission-line region (ELG), low-ionization narrow emission-line region (LINER), spiral or irregular (SPIRR) and finally, elliptical and S0 (E/S0) galaxies.

3 TREATMENT OF THE DATA

In Table 1, we present, separated by galaxy class, the redshifts, X-ray and 60-μm luminosities and *IRAS* colours. The sources of these data are listed in the right-most column. X-ray luminosities in Table 1 have been converted to the 0.5–4.5 keV bandpass when necessary (see below). The number of galaxies in each class can be seen in Table 2 under redshift (z). Throughout this paper, luminosities (in erg s^{-1}) are calculated from fluxes (in units of erg cm^{-2} s^{-1}) for a Hubble constant of $H_0 = 50$ km s^{-1} Mpc^{-1} and $q_0 = 0$. We use the convention that monochromatic flux density $f_\nu \propto \nu^\alpha$. For purposes of comparison, the reader should be aware that many X-ray studies have adopted $f_X \propto \nu^{-\alpha_X}$. Upper limits for all data are quoted at the 3σ level.

We make some limited use of data other than from *IRAS* and *Einstein*. Since redshift is used in the X-ray flux integral in conjunction with N_H absorption cross-sections, we use redshifts listed in the original X-ray reference, and scale luminosities to $H_0 = 50$ km s^{-1} Mpc^{-1} when necessary. We classify objects with $M_B < -23.1$ as quasars, using blue magnitudes or $B-V$ colours taken from Véron-Cetty & Véron (1987) or from the X-ray references.

3.1 Infrared data

For most galaxies, we use *IRAS* fluxes as listed in the Point Source Catalog (PSC, 1985). However, the sensitivity of the *IRAS* all-sky survey is such that very few quasars in the PSC were detected. For this reason, for most quasars we use data from *IRAS* coadded scans (Sanders *et al.* 1989) and from pointed observations (Neugebauer *et al.* 1986). These data are calibrated to the same absolute scale as the PSC, yet boast increases in sensitivity over the PSC by factors of about 5 and 3, respectively. *IRAS* quasar data for which confusion or infrared cirrus is indicated have been excluded from the statistical analysis.

A conservatively large galaxian disc (35 kpc in diameter) fits into the smallest *IRAS* aperture only at distances greater than 160 Mpc ($H_0 = 50$ km s^{-1} Mpc^{-1}). Since *IRAS* apertures may begin to exclude some flux from nearer galaxies, we obtained coadded data for all galaxies nearer than this distance for use in our analysis. *IRAS* coadded data were reduced at the Infrared Processing and Analysis Center

Table 1. X-ray and infrared data.

QUASARS

Object Name	Coordinates	z	logL_X (0.5-4.5keV)	log$L_{60\mu m}$	log$\frac{L_X}{L_{60\mu m}}$	$\alpha(25,60)$	$\alpha(60,100)$	$\alpha(12,60)$	References
PHL658	0003+158	0.450	45.610	<45.626	>-0.016	...	...	...	3X,4I
IIIZW2	0008+107	0.089	44.669	44.594	0.075	-0.306	...	-0.476	6X,4I
3CR9	0017+154	2.012	45.940	<47.421	>-1.481	...	...	...	7X,4I
PG0026	0026+129	0.142	44.878	<44.123	>0.756	...	...	...	5X,4I
PKS0044	0044+030	0.624	45.400	<46.680	>-1.280	...	...	...	3X,17I
IZw1	0051+124	0.060	44.322	45.273	-0.950	-0.842	-0.499	-0.888	6X,4I
PG0052	0052+251	0.155	44.980	44.741	0.239	<0.754	>-2.526	<-0.094	3X,4I
PHL909	0054+144	0.171	44.687	45.376	-0.689	-1.392	-1.965	-0.868	5X,4I
PHL957	0100+130	2.681	<46.540	<47.303	...	...	...	...	9X,4I
PKS0109	0109+176	2.157	<46.190	<47.386	...	...	...	...	9X,4I
PG0117	0117+213	1.493	45.905	<47.356	>-1.451	...	...	...	3X,17I
MKN1014	0157+001	0.163	44.250	46.207	-1.957	-1.736	0.046	-1.773	3X,17I
PKS0229	0229+131	2.065	46.738	<46.945	>-0.208	...	...	...	18X,4I
4C28.07	0234+285	1.207	46.218	47.144	-0.926	<-1.207	...	<-1.041	18X,4I
PKS0312	0312-770	0.223	44.983	<44.905	>0.078	...	...	...	5X,4I
PKS0420	0420-012	0.915	46.120	47.103	-0.983	-1.234	-1.438	<-1.481	9X,4I
PKS0438	0438-436	2.852	46.860	48.034	-1.174	<-1.662	-1.652	-0.975	7X,4I
PKS0537	0537-441	0.894	45.780	47.279	-1.499	-0.857	-0.484	-0.897	7X,4I
OH471	0642+449	3.400	47.200	<47.902	>-0.702	...	...	...	7X,4I
3CR175	0710+118	0.768	45.340	<46.117	>-0.777	...	...	...	7X,4I
PKS0736	0736+014	0.191	44.440	45.091	-0.651	-0.624	...	-0.848	9X,4I
3C190	0758+143	1.197	<45.400	<46.760	...	...	...	...	30X,4I
PG0804	0804+761	0.100	44.760	44.652	0.108	0.103	>-0.979	-0.003	3X,17I
VIIZW244	0838+770	0.131	43.960	44.865	-0.905	-0.599	-1.753	-1.014	3X,4I
4C39.25	0923+392	0.698	45.881	<45.689	>0.192	...	...	...	5X,4I
PG1001	1001+054	0.161	<43.620	44.239	<-0.619	0.329	>-1.837	0.086	3X,4I

Table 1 – *continued*

Object Name	Coordinates	z	$\log L_X$ (0.5-4.5keV)	$\log L_{60\mu m}$	$\log \frac{L_X}{L_{60\mu m}}$	$\alpha(25,60)$	$\alpha(60,100)$	$\alpha(12,60)$	References
PG1004	1004+130	0.240	<43.670	45.464	<-1.794	<-0.276	>-0.777	<-0.461	3X,4I
PG1008	1008+133	1.280	<45.660	<47.088	. . .	>0.274	. . .	>-0.046	3X,17I
PKS1048	1048-090	0.344	<45.660	<47.088	. . .	>0.274	. . .	>-0.046	3X,17I
3CR249.1	1100+772	0.311	45.330	<45.719	>-0.389	. . .	. . .	. . .	5X,4I
MKN1298	1126-041	0.060	45.309	45.218	0.092	-0.347	. . .	-0.794	3X,4I
PG1138	1138+040	1.876	42.690	44.740	-2.050	-0.882	-1.098	-1.157	3X,17I
3CR263	1137+660	0.652	45.830	<45.991	>-0.161	. . .	. . .	. . .	5X,4I
PG1202	1202+281	0.165	44.934	44.870	0.064	0.137	-2.623	<-0.072	5X,17I
PKS1207	1206-399	0.966	45.630	<46.422	>-0.792	. . .	<-3.607	. . .	7X,4I
PG1211	1211+143	0.085	44.746	44.693	0.053	0.196	-1.595	-0.356	5X,4I
PG1216	1216+069	0.334	45.090	<45.690	>-0.600	. . .	. . .	. . .	3X,17I
TON1530	1222+228	2.046	46.025	<47.665	>-1.640	. . .	. . .	. . .	3X,17I
B1225	1225+317	2.220	46.680	<47.387	>-0.707	. . .	. . .	. . .	7X,4I
3C273	1226+023	0.158	45.987	46.044	-0.057	-0.744	-1.064	-0.910	5X,4I
PG1241	1241+176	1.273	45.800	<47.123	>-1.323	. . .	. . .	. . .	3X,17I
PKS1302	1302-102	0.286	45.290	<45.576	>-0.286	. . .	. . .	. . .	3X,17I
PG1307	1307+085	0.155	44.738	<44.960	>-0.221	. . .	. . .	. . .	5X,17I
PG1333	1333+176	0.554	45.050	<46.160	>-1.110	. . .	. . .	. . .	3X,17I
PG1351	1351+640	0.088	43.150	45.123	-1.973	-0.403	-0.876	-0.917	7X,4I
PB4142	1352+183	0.158	44.690	<44.936	>-0.246	. . .	. . .	. . .	3X,17I
PG1352	1352+011	1.121	<45.580	<46.974	. . .	. . .	. . .	. . .	3X,17I
TON182	1402+266	0.164	44.420	45.185	-0.765	<-0.869	-0.774	-0.736	3X,17I
PG1407	1407+265	0.944	46.309	<46.736	>-0.427	. . .	. . .	. . .	5X,17I
PG1416	1416-129	0.129	44.978	<44.749	>0.229	. . .	. . .	. . .	5X,17I
TON202	1425+267	0.366	44.770	<45.653	>-0.883	. . .	. . .	. . .	3X,17I
MKN1383	1426+015	0.086	44.498	44.738	-0.239	-0.709	>0.019	-0.585	5X,4I
PG1435	1435-067	0.129	44.630	<44.704	>-0.074	. . .	. . .	. . .	3X,17I
OQ172	1442+101	3.530	47.060	. . .	. . .	. . .	. . .	. . .	9X,4I
PG1519	1519+226	0.137	44.250	<44.708	>-0.458	. . .	. . .	. . .	3X,17I
KP57	1544+212	2.050	<46.220	<47.193	. . .	. . .	. . .	. . .	9X,4I
KP58	1545+209	1.850	<46.080	<47.063	. . .	. . .	. . .	. . .	9X,4I
3C323.1	1545+210	0.266	45.372	. . .	. . .	. . .	. . .	. . .	5X,4I
KP59	1545+210	1.890	<46.110	. . .	. . .	. . .	. . .	. . .	9X,4I
MC1548A	1548+115	0.436	45.460	45.587	-0.127	<-0.489	>-5.293	<-0.470	7X,4I
PG1552	1552+085	0.119	<43.640	<44.630	. . .	. . .	. . .	>-0.113	3X,17I
KP67	1606+289	2.56	<46.110	<47.208	. . .	. . .	. . .	. . .	9X,17I
NAB1612	1612+266	0.395	44.400	<45.401	>-1.001	. . .	. . .	. . .	9X,4I
TON256	1612+261	0.131	44.660	<44.350	>0.310	. . .	. . .	. . .	3X,4I
MKN876	1613+658	0.129	44.708	45.418	-0.710	-1.155	-1.058	-1.235	6X,4I
MKN877	1617+175	0.114	44.096	<44.482	>-0.385	. . .	. . .	. . .	6X,17I
4C38.41	1633+382	1.814	46.230	46.923	-0.693	<-1.354	>-1.411	<-0.544	9X,4I
PG1634	1634+703	1.334	46.160	47.387	-1.227	-0.881	-0.148	-1.026	3X,4I
3C345	1641+399	0.594	45.960	46.983	-1.023	-0.935	-1.001	-1.039	9X,4I
3C351	1704+608	0.371	44.970	45.868	-0.898	-0.435	. . .	-0.858	7X,4I
3C380	1828+487	0.691	45.940	45.906	0.034	-0.390	-2.714	-0.368	7X,4I
MKN509	2041-109	0.035	44.005	44.609	-0.604	-0.932	-0.124	-0.908	20X,4I
PG2112	2112+059	0.466	<44.770	45.856	<-1.086	-0.415	>-1.022	-0.243	3X,4I
PKS2126	2126-158	3.275	47.760	48.067	-0.307	<-0.042	>-1.618	<-0.402	7X,4I
IIZW136	2130+099	0.063	44.169	44.637	-0.468	-0.273	. . .	-0.582	6X,4I
OX169	2141+175	0.213	44.200	<45.078	>-0.878	. . .	<-2.784	>-0.803	7X,4I
MKN304	2214+139	0.067	43.480	44.539	-1.059	-1.446	. . .	-1.062	6X,4I
3C446	2223-052	1.404	46.980	48.119	-1.139	-1.100	-1.190	-1.077	7X,4I
PG2233	2233+134	0.325	44.670	<45.663	>-0.993	. . .	. . .	. . .	3X,17I

Table 1 – *continued*

Object Name	Coordinates	z	$\log L_X$ (0.5-4.5keV)	$\log L_{60\mu m}$	$\log \frac{L_X}{L_{60\mu m}}$	$\alpha(25,60)$	$\alpha(60,100)$	$\alpha(12,60)$	References
PKS2251	2251+113	0.323	44.160	<45.296	>-1.136	. . .	. . .	. . .	3X,4I
PKS2344	2344+092	0.677	45.770	46.051	-0.281	0.066	. . .	<-0.783	7X,4I
PKS2345	2345-167	0.576	45.240	46.065	-0.825	<0.012	>-1.038	<-0.424	9X,4I
PKS2349	2349-014	0.174	44.969	45.313	-0.344	<-0.467	>-0.133	<-0.511	6X,17I
				SEYFERT 1 GALAXIES					
MKN334	0000+2140	0.022	<41.763	44.640	<-2.877	-1.616	-0.080	<-1.742	1XI,16D
MKN335	0003+1955	0.026	44.370	43.584	0.786	0.693	>-0.865	-0.050	1XI,44D
MKN1148	0049+1709	0.064	44.310	<44.169	>0.141	. . .	. . .	. . .	3X,17I
IIZW1	0119-0118	0.054	43.274	<44.998	>-1.724	>-1.352	. . .	>-1.101	6X,1I
MKN357	0119+2254	0.053	<42.800	44.797	<-1.997	<-1.530	>-0.054	<-0.446	3X,1I
MKN359	0124+1855	0.017	43.070	43.918	-0.848	-0.722	-1.110	-0.968	1XI,16D
MKN590	0212-0100	0.027	43.572	43.937	-0.364	<-0.389	-1.986	<-0.355	6X,1I
AKN81	0220+3158	0.035	<42.103	45.275	<-3.172	-2.573	-1.330	<-1.967	1XI,16D
MKN1040	0225+3105	0.016	43.563	44.212	-0.648	-0.800	-1.259	-1.065	6X,1I
MKN1048	0232-0900	0.043	44.099	44.779	-0.680	-1.104	-0.643	<-1.052	6X,1I
NGC1365	0331-3618	0.005	41.148	44.711	-3.563	-2.258	-1.053	-1.906	6X,1I
1E0412	0412-0803	0.039	43.181	44.352	-1.171	-0.220	>-0.825	<-0.575	24X,1I
NGC1566	0418-5503	0.004	41.653	43.947	-2.294	-2.360	-1.897	-1.466	6X,1I
3C120	0430+0514	0.033	44.233	44.501	-0.268	-0.700	-1.372	-0.857	6X,1I
MKN618	0434-1028	0.035	43.702	44.870	-1.168	-1.425	-0.767	-1.317	6X,1I
IRAS0459	0459-2257	0.041	42.810	44.485	-1.675	-1.266	-1.357	<-0.668	2X,1I
AKN120	0513-0012	0.033	44.453	44.189	0.264	-0.375	-1.336	<-0.313	6X,1I
M8-11-11	0551+4625	0.021	43.689	44.488	-0.799	-0.492	-0.806	-0.945	20X,1I
MKN376	0710+4547	0.056	44.490	44.798	-0.308	-0.477	>-0.816	<-0.568	8X,1I
MKN9	0732+5852	0.040	43.593	44.486	-0.893	-0.587	-0.927	<-0.688	6X,1I
MKN79	0738+4955	0.022	43.680	44.251	-0.571	-1.296	-0.592	-1.059	8X,1I
MKN704	0915+1631	0.029	43.539	<43.964	>-0.425	>0.240	. . .	>-0.158	6X,1I
MKN705	0923+1256	0.029	43.560	44.105	-0.545	<-0.939	>-1.691	<-0.628	3X,1I
NGC3227	1020+2007	0.005	42.527	43.659	-1.131	-1.858	-1.527	-1.309	6X,1I
PG1011	1011-0403	0.058	42.580	44.102	-1.522	<-0.418	>-0.853	<-0.390	3X,17I
NGC3516	1103+7250	0.009	42.414	43.527	-1.112	-0.823	-0.470	-1.208	6X,1I
MKN734	1119+1200	0.049	43.710	44.466	-0.756	-0.763	-0.611	-0.941	3X,17I
NGC3783	1136-3727	0.010	43.282	43.879	-0.597	-0.435	-0.858	-0.802	6X,1I
NGC4051	1200+4448	0.002	41.800	43.075	-1.275	-1.720	-1.881	-1.250	31X,1I
NGC4151	1208+3941	0.003	41.520	43.198	-1.678	-0.433	-0.483	-0.729	19X,27I
NGC4235	1214+0727	0.008	42.732	42.677	0.055	<-0.874	-1.325	<-0.701	6X,27I
MKN766	1215+3005	0.013	42.340	44.135	-1.795	-1.168	-0.241	-1.592	8X,1I
MKN205	1219+7535	0.070	44.428	<44.661	>-0.234	. . .	<-2.277	. . .	6X,1I
TON1542	1229+204	0.064	44.160	44.190	-0.030	0.704	>-2.039	<-0.206	3X,17I
NGC4579	1235+1205	0.004	40.674	43.343	-2.669	-2.311	-2.634	-0.969	10X,1I
PG1244	1244+026	0.048	43.930	44.167	-0.237	<-1.176	>-0.231	<-0.542	3X,17I
MKN231	1254+5708	0.041	<42.158	46.101	<-3.944	-1.567	0.164	-1.815	26X,1I
IIZW10	1310-108	0.034	43.484	<43.601	>-0.117	. . .	. . .	. . .	6X,17I
IC4329A	1346-3003	0.014	43.933	43.988	-0.054	-0.109	0.034	-0.481	20X,1I
MKN279	1351+6933	0.030	43.891	44.341	-0.450	-1.635	-1.463	<-0.904	6X,1I
PG1404	1404+226	0.098	43.240	<44.553	>-1.313	. . .	. . .	. . .	3X,17I
NGC5548	1415+2522	0.017	43.429	43.768	-0.339	-0.362	-1.386	-0.413	20X,1I
MKN474	1432+4853	0.044	43.410	44.315	-0.905	<-0.721	-2.051	<-0.392	8X,1I
IRAS1443	1443+2714	0.029	41.700	44.163	-2.463	-0.949	-0.819	<-0.712	2X,1I
MKN841	1501+1037	0.036	44.111	44.159	-0.048	-0.137	>1.052	-0.929	6X,17I
MKN290	1534+5804	0.030	43.708	<43.512	>0.196	>0.147	. . .	>-0.298	6X,17I
MKN507	1748+6843	0.055	42.998	44.552	-1.554	<-0.812	-1.036	<-0.442	6X,1I
E140-G43	1840-6224	0.014	43.340	44.010	-0.670	-1.067	-0.111	-0.946	8X,1I

Table 1 – *continued*

Object Name	Coordinates	z	$\log L_X$ (0.5-4.5keV)	$\log L_{60\mu m}$	$\log \frac{L_X}{L_{60\mu m}}$	$\alpha(25,60)$	$\alpha(60,100)$	$\alpha(12,60)$	References
3C390.3	1845+7943	0.056	44.363	<44.456	>-0.092	>-0.360	. . .	. . .	6X,1I
E141-G55	1916-5845	0.037	44.366	44.277	0.089	-0.653	>-3.990	-0.564	20X,1I
NGC6814	1939-1026	0.005	41.609	43.647	-2.038	-2.178	-2.062	-1.092	6X,1I
MKN896	2043-0259	0.026	43.153	43.928	-0.775	<-1.689	-1.385	<-1.037	1XI,16D
PKS2048	2048-5715	0.011	41.478	44.202	-2.723	-0.443	1.120	-0.964	1XI,16D
NGC7213	2206-4724	0.005	42.964	43.246	-0.282	-1.356	-2.397	-0.847	6X,1I
NGC7469	2300+0836	0.016	43.400	45.212	-1.811	-1.860	-0.441	-1.802	6X,1I
MKN315	2301+2221	0.039	43.645	44.705	-1.059	-1.582	>-1.256	<-0.833	6X,1I
MKN530	2316-0001	0.030	43.334	44.208	-0.873	<-0.639	-1.833	<-0.516	6X,1I
			SEYFERT 2 GALAXIES						
MKN348	0046+3141	0.015	41.557	43.866	-2.309	-0.436	0.427	-1.024	6X,1I
Tol0109	0109-3820	0.011	41.600	43.704	-2.104	-0.131	0.224	-0.304	33X,1I
MKN1	0113+3249	0.016	<41.260	44.198	<-2.938	-1.243	-0.210	-0.591	8X,1I
NGC513	0121+3332	0.019	41.233	44.287	-3.054	-1.767	-1.035	-1.745	1XI
IRAS0121	0121+0122	0.138	<43.223	46.033	<-2.810	-1.924	-0.280	<-1.354	1XI,34D
IRAS0135	0135-1307	0.040	<42.480	44.536	<-2.056	-0.823	-0.449	<-0.457	2X,1I
IRAS0147	0147+3554	0.080	<42.850	44.979	<-2.129	-0.748	>-0.968	<-0.557	2X,1I
MKN573	0141+0205	0.017	41.482	43.895	-2.413	-0.541	-0.123	-0.868	6X,1I
NGC1068	0240-0013	0.004	41.849	44.850	-3.002	-0.949	-0.412	-0.976	6X,1I
IIIZW55	0338-0127	0.025	<41.800	44.187	<-2.387	-1.081	-1.366	<-1.582	8X,1I
NGC1685	0450-0301	0.015	<41.383	43.753	<-2.370	<-2.888	-1.031	<-1.286	1XI,16D
NGC2110	0549-0728	0.008	42.163	43.768	-1.604	-2.289	-0.665	-1.614	6X,1I
MKN3	0609+7103	0.014	41.857	44.188	-2.331	-0.447	0.656	-0.973	6X,1I
MKN78	0737+6517	0.037	42.298	44.532	-2.234	-0.833	-0.183	<-0.932	6X,1I
NGC2992	0943-1405	0.008	43.164	44.125	-0.962	-2.556	-0.525	-1.857	6X,1I
NGC3281	1029-3435	0.011	<41.263	44.278	<-3.014	-1.162	-0.122	-1.252	1XI,16D
MKN34	1030+6017	0.051	<42.490	44.761	<-2.271	-0.804	>-0.357	<-0.805	8X,1I
IRAS1050	1050-1843	0.054	<42.443	45.463	<-3.020	-2.504	-0.534	<-1.641	1XI,34D
MKN1291	1121-0823	0.011	41.510	43.737	-2.227	-1.536	-1.547	<-1.525	40X,1I
MKN176	1129+5313	0.027	<41.800	44.053	<-2.253	-1.535	>-1.343	<-0.539	8X,1I
MKN198	1206+4720	0.024	<41.970	43.921	<-1.951	-1.490	-0.217	<-1.077	8X,1I
NGC4388	1223+1256	0.004	40.750	43.632	-2.882	-1.214	-1.064	-1.472	2X,1I
NGC4507	1232-3938	0.012	41.600	44.117	-2.517	-1.523	-0.630	-1.527	6X,1I
IRAS1254	1254-3006	0.055	<43.340	44.834	<-1.494	-1.155	-0.839	<-0.855	2X,1I
NGC5135	1322-2934	0.013	41.339	44.808	-3.469	-2.257	-1.148	-2.199	14X,1I
MKN268	1338+3037	0.041	<42.133	44.742	<-2.609	<-1.850	-0.440	<-1.084	1XI,16D
MKN273	1342+5608	0.037	42.506	45.878	-3.372	-2.650	0.118	-2.695	6X,1I
PG1345	1345+1232	0.121	<43.153	45.848	<-2.695	-1.263	-0.123	<-1.295	1XI,43D
MKN463E	1353+1836	0.050	42.170	45.069	-2.900	-0.346	0.300	-0.837	6X,1I
NGC5506	1410-0258	0.007	42.927	43.947	-1.020	-0.804	0.043	-1.181	6X,1I
NGC5643	1429-4357	0.003	40.469	43.742	-3.273	-1.863	-1.217	-1.526	14X,1I
NGC5674	1431+0540	0.025	42.183	44.337	-2.153	-2.064	-1.621	-1.535	6X,1I
MKN477	1439+5343	0.038	<42.110	44.638	<-2.528	-1.053	-0.617	<-1.048	8X,1I
NGC5728	1439-1702	0.010	41.129	44.255	-3.126	-2.468	-1.201	-2.135	14X,1I
1E1530	1530-0831	0.023	41.890	44.387	-2.497	-1.547	-0.756	-1.090	21X,1I
ARP220	1532+2340	0.018	41.518	45.900	-4.383	-2.977	-0.165	-3.212	26X,1I
3C327	1559+0206	0.104	43.193	45.189	-1.996	-0.794	>-1.111	<-0.406	1XI,16D
IRAS1729	1729+5940	0.028	<41.910	44.086	<-2.176	-2.310	-1.906	<-0.627	2X,1I
ESO103-G3	1833-6528	0.016	<43.360	44.076	<-0.716	0.044	1.184	-0.851	2X,1I,44D
NGC7496	2306-4341	0.005	41.694	43.681	-1.986	-1.775	-1.101	-1.480	6X,1I
NGC7582	2315-4238	0.005	41.787	44.427	-2.640	-2.258	-0.915	-1.954	6X,1I
NGC7590	2316-4230	0.005	40.506	43.663	-3.158	-2.373	-1.789	-1.424	35X,1I
IRAS2346	2346+0157	0.031	<42.270	44.585	<-2.315	-1.190	-0.830	<-1.227	2X,1I

Table 1 – *continued*

Object Name	Coordinates	Distance (Mpc)	$\log L_X$ (0.5-4.5keV)	$\log L_{60\mu m}$	$\log \frac{L_X}{L_{60\mu m}}$	$\alpha(25,60)$	$\alpha(60,100)$	$\alpha(12,60)$	References
			EMISSION LINE GALAXIES						
ESO0350	0034-3349	118.8	<41.760	44.738	<-2.978	-1.134	0.505	-1.601	2X,1I
NGC253	0045-2533	5.2	40.110	44.209	-4.099	-2.123	-1.219	-1.792	12X,15I
NGC520	0121+0331	46.5	40.810	44.637	-3.827	-2.710	-0.739	-2.207	10X,1I
MKN1022	0207-1023	77.5	41.410	44.762	-3.352	-2.448	0.212	-2.067	2X,1I
NGC839	0207-1025	77.5	<41.140	44.603	<-3.463	-1.782	-1.216	-1.935	2X,1I
NGC1313	0317-6640	4.8	39.580	42.696	-3.116	-2.665	-1.838	-2.258	12X,15I
IC342	0341+6756	4.6	39.850	43.511	-3.661	-1.980	-1.859	-1.480	12X,15I
NGC1559	0417-6253	20.5	40.180	43.857	-3.677	-2.591	-1.557	-1.795	12X,1I
VIIZw16	0426+6444	3.7	39.278	42.650	-3.372	-2.071	-0.067	-2.341	6X,1I
MKN617	0431-0840	94.3	41.725	45.258	-3.533	-1.741	-0.053	-1.942	6X,1I
NGC1672	0444-5920	23.0	40.686	44.113	-3.427	-2.359	-1.320	-1.255	6X,1I
IRAS0833	0833+6517	112.9	41.490	44.680	-3.190	-1.917	-0.262	<-1.904	28X,1I
ARP215	0910+4019	50.8	41.428	44.174	-2.746	-2.223	-0.797	-1.571	41X,1I
NGC2903	0929+2143	9.3	39.980	43.434	-3.454	-2.199	-2.025	-1.460	12X,15I
M82	0951+6954	3.2	40.152	43.905	-3.753	-1.708	-0.119	-1.832	42X,15I
MKN133	0957+7222	43.8	<41.280	43.582	<-2.302	-1.809	-1.210	-1.355	36X,1I
NGC3077	0959+6858	3.2	38.280	41.965	-3.685	-2.220	-1.182	-1.913	10X,1I
Tol3	1004-2941	22.0	40.260	43.173	-2.913	-2.451	-0.577	-2.065	13X,1I
NGC3265	1028+2903	24.0	<40.300	42.917	<-2.617	-2.126	-0.634	<-2.209	2X,1I
NGC3310	1035+5345	21.0	40.610	43.973	-3.363	-2.186	-0.525	-1.920	13X,1I
NGC3368	1044+1205	16.0	39.850	43.188	-3.338	-3.290	-2.108	-1.495	10X,1I
NGC3448	1051+5434	29.0	40.430	43.510	-3.080	-2.706	-1.175	-2.040	13X,1I
ARP281	1239+3249	12.1	40.290	43.840	-3.550	-2.658	-1.334	-1.703	23X,1I
NGC5204	1327+5840	7.2	39.620	41.959	-2.339	<-4.282	-1.327	<-2.237	25X,1I
M83	1333-2937	6.7	40.200	43.557	-3.357	-2.548	-1.710	-1.857	12X,1I
NGC5253	1337-3123	4.0	38.380	42.482	-4.102	-1.091	0.154	-1.542	12X,1I
NGC5408	1400-4108	8.0	40.017	42.095	-2.077	-2.375	-0.228	<-1.858	29X,1I
M101	1401+5433	7.2	40.150	43.437	-3.287	-2.297	-2.065	-1.649	10X,15I
HARO40	1407+2636	349.8	<42.810	44.888	<-2.078	-1.596	-0.466	<-0.819	2X,1I
IRAS1521	1521+0843	218.0	<42.230	44.390	<-2.160	-0.948	>-0.544	<-0.707	2X,1I
NGC6744	1905-6354	10.4	40.150	42.934	-2.784	<-1.864	-2.644	<-2.492	12X,1I
IC4870	1932-6555	18.0	<39.923	42.012	<-2.089	-0.954	>-0.774	-0.975	1XI,16D
NGC6946	2033+6000	7.0	39.990	43.604	-3.614	-2.130	-1.809	-1.505	13X,15I
IRAS2045	2045+0013	71.6	<41.070	43.638	<-2.568	-1.109	>0.578	-1.300	2X,1I
NGC7552	2313-4251	32.7	40.919	44.697	-3.778	-2.098	-0.621	-1.905	14X,1I
MKN538	2333+0152	57.7	41.120	44.313	-3.193	-1.680	-0.271	-2.128	14X,1I
NGC7793	2355-3252	3.2	39.200	42.080	-2.880	-2.558	-2.065	-1.581	10X,15I
			LINER GALAXIES						
NGC1052	0238-0828	29.8	40.853	42.705	-1.852	-0.448	-1.251	-1.123	1XI,16D
NGC1097	0244-3029	24.5	41.080	44.228	-3.148	-2.060	-1.786	-1.731	10X,15I
NGC2841	0918+5111	12.0	39.980	42.582	-2.602	-1.908	-3.334	-0.987	10X,15I
M81	0951+6918	3.5	40.230	42.516	-2.286	-2.411	-2.659	-1.263	37X,15I
NGC3079	0958+5555	30.0	40.963	44.441	-3.478	-3.074	-1.429	-1.828	6X,1I
ARP120	1225+1317	25.7	39.940	43.234	-3.294	-3.828	-2.026	-2.004	38X,15I
M90	1234+1326	25.7	40.635	43.605	-2.970	-1.908	-1.896	-1.215	6X,1I
M104	1237-1120	19.3	40.940	42.949	-2.009	-1.876	-2.733	-0.882	10X,1I
NGC4826	1254+2157	5.0	39.460	42.740	-3.280	-2.876	-1.547	-1.705	10X,1I
NGC6764	1907+5051	47.8	<40.930	43.983	<-3.053	-1.837	-1.273	-1.645	8X,1I
			SPIRAL and IRREGULAR GALAXIES						
NGC247	0044-2101	3.4	39.200	41.739	-2.539	<-4.458	-2.421	<-2.604	10X,15I
M33	0131+3024	0.7	38.920	42.090	-3.170	-2.677	-2.147	-1.586	10X,15I
M74	0134+1532	17.2	40.110	43.570	-3.460	-2.737	-2.244	-1.435	10X,15I

Table 1 – *continued*

Object Name	Coordinates	Distance (Mpc)	$\log L_X$ (0.5-4.5keV)	$\log L_{60\mu m}$	$\log \frac{L_X}{L_{60\mu m}}$	$\alpha(25,60)$	$\alpha(60,100)$	$\alpha(12,60)$	References
NGC1073	0241+0109	26.4	40.230	43.047	-2.817	-3.036	-2.231	<-2.072	10X,1I
NGC1300	0317-1935	30.4	<40.540	43.330	<-2.790	-1.813	-2.362	-1.426	10X,1I
NGC1350	0329-3347	29.3	<40.530	42.647	<-2.117	-1.791	-3.525	-0.911	10X,1I
NGC1398	0336-2629	30.4	40.490	43.117	-2.627	-1.981	-3.083	-0.941	10X,1I
MKN71	0723+6917	3.2	<38.510	41.451	<-2.941	-2.220	-0.353	<-0.890	10X,1I
NGC2403	0732+6543	3.2	39.380	42.500	-3.120	-2.403	-2.071	-1.700	10X,15I
NGC2763	0904-1517	10.7	39.380	42.197	-2.817	-2.724	-1.892	-1.479	10X,1I
NGC2775	0907+0714	19.3	40.150	42.771	-2.621	-1.977	-2.801	-1.035	10X,1I
NGC2848	0917-1618	10.7	<39.320	42.058	<-2.738	-2.357	-2.357	-1.633	10X,1I
NGC3593	1111+1305	16.0	39.930	43.475	-3.545	-2.601	-1.285	-1.603	10X,1I
NGC3628	1117+1351	16.0	40.790	43.874	-3.084	-2.529	-1.808	-1.713	10X,15I
NGC4236	1214+6941	3.2	38.820	41.388	-2.568	-2.220	-1.807	-2.230	10X,15I
NGC4244	1215+3804	5.0	39.040	41.799	-2.759	<-4.677	-2.626	<-2.753	10X,15I
NGC4378	1222+0512	47.8	<41.293	43.013	<-1.720	<-1.487	-1.642	-0.295	1XI,39D
NGC5068	1316-2046	7.9	39.480	42.578	-3.098	-2.732	-2.024	-1.185	10X,1I
NGC5078	1317-2708	7.9	39.110	42.603	-3.493	-3.025	-2.286	-1.375	10X,1I
NGC5101	1319-2709	7.9	<39.530	41.626	<-2.096	<-2.682	-2.470	-1.014	10X,1I
NGC5566	1417-2901	34.6	<40.710	43.160	<-2.450	<-2.822	-1.778	-1.344	10X,1I
NGC5907	1514+5629	18.4	40.340	43.253	-2.913	-2.139	-3.232	-1.226	10X,15I
			ELLIPTICAL/S0 GALAXIES						
NGC524	0122+0916	48.5	40.830	43.044	-2.214	<-1.764	-2.008	-1.161	11X,1I
NGC1316	0320-3723	32.6	41.590	43.328	-1.738	-2.455	-1.912	<-1.093	22X,1I
NGC1332	0324-2130	30.4	40.740	42.427	-1.687	-1.622	-2.369	-0.482	11X,1I
NGC1380	0334-3508	26.2	40.550	42.661	-2.111	<-3.475	-2.383	-0.403	11X,1I
NGC1400	0337-1851	10.4	<39.210	41.703	<-2.493	<-2.502	-2.308	<-1.199	11X,1I
NGC1533	0408-5614	19.8	39.760	41.873	-2.113	-0.371	-2.792	<-0.782	11X,1I
NGC2685	0851+5856	25.0	39.910	42.299	-2.389	-1.437	-2.357	-1.150	11X,1I
NGC2974	0940-0328	42.9	40.690	42.620	-1.930	-1.419	-2.542	-0.093	11X,1I
NGC4203	1212+3328	30.0	41.340	42.569	-1.229	-1.594	-2.582	<-0.966	11X,1I
NGC4459	1226+1415	25.7	40.090	42.839	-2.749	<-2.203	-1.978	-0.654	11X,1I
NGC4477	1227+1354	25.7	40.030	42.261	-2.231	-0.396	-0.886	-0.635	11X,1I
NGC4643	1240+0215	25.7	40.170	42.464	-2.294	-2.183	-2.509	-1.315	11X,1I
NGC4753	1249-0055	25.7	40.090	43.443	-3.353	-2.577	-0.573	-1.768	11X,1I
NGC5102	1319-3622	3.4	<38.630	40.754	<-2.124	<-2.019	-2.355	<-1.307	11X,15I
NGC5128	1322-4245	2.0	39.300	42.717	-3.417	-2.235	-1.634	-1.395	11X,15I
NGC5866	1505+5557	25.5	40.190	43.330	-3.140	-3.123	-2.261	-1.687	11X,1I
IC1459	2254-3643	27.5	40.480	42.425	-1.945	-0.282	-1.104	-0.773	11X,1I

X = X-ray data, *I* = *IRAS* data, *D* = redshift. (1) This paper; (2) Green *et al.* 1989; (3) Tananbaum *et al.* 1986; (4) Neugebauer *et al.* 1986; (5) Wilkes & Elvis 1987; (6) Kruper, Urry & Canizares 1990; (7) Zamorani *et al.* 1981; (8) Kriss, Canizares & Ricker 1980; (9) Ku, Helfand & Lucy 1980; (10) Long & Van Spreybroeck 1983; (11) Canizares, Fabbiano & Trinchieri 1987; (12) Fabbiano, Trinchieri & MacDonald 1984; (13) Fabbiano, Feigelson & Zamorani 1982; (14) Phillips, Charles & Baldwin 1983; (15) Rice *et al.* 1988; (16) Véron-Cetty & Véron 1987; (17) Sanders *et al.* 1989; (18) Owen, Helfand & Spangler 1981; (19) Lawrence & Elvis 1982; (20) Petre *et al.* 1984; (21) Reichert *et al.* 1982; (22) Trinchieri & Fabbiano 1985; (23) Fabbiano, Gioia & Trinchieri 1988; (24) Steiner, Grindlay & Maccacaro 1982; (25) Fabbiano & Panagia 1983; (26) Eales & Arnaud 1988; (27) Edelson, Malkan & Rieke 1987; (28) Margon *et al.* 1988; (29) Stewart *et al.* 1982; (30) Bregman *et al.* 1985; (31) Marshall *et al.* 1983a,b; (32) Ward *et al.* 1988; (33) Fosbury & Sansom 1983; (34) Heckman, Armus & Miley 1987; (35) Maccacaro & Perola 1981; (36) Ulvestad & Wilson 1983; (37) Elvis & Van Spreybroeck 1982; (38) Forman *et al.* 1979; (39) Véron-Cetty & Véron 1986; (40) Kollatschny *et al.* 1983; (41) Kinney *et al.* 1984; (42) Watson, Stanger & Griffiths 1984; (43) Burg & Huchra, in preparation; (44) Steiner 1981.

Table 2. Univariate results: means and two-sample tests.

OPTICAL CLASSIFICATIONS

Parameter	Class	Sample Total	Sample Limits	Sample Deleted	Median	Mean	Error	Trunc?	Probability (%) Gehan	Probability (%) Logrank	Versus	Notes
log z	QSO	83	0	0	-0.4	-0.4	.06	N	<0.01	<0.01	SY1	
	SY1	57	0	0	-1.5	-1.6	.05	N	18.6	76.2	SY2	
	SY2	43	0	0	-1.7	-1.7	.06	N	<0.01	<0.01	ELG	
	LIN	10	0	0	-2.4	-2.5	.11	N	18.6	13.5	SPIRR	
	ELG	37	0	0	-2.5	-2.5	.09	N	13.0	5.0	SPIRR	
	SPIRR	22	0	0	-2.6	-2.8	.09	N	4.3	11.6	E/S0	
	E/S0	17	0	0	-2.4	-2.5	.09	N				
$\log L_X$	QSO	83	14U	0	45.0	45.1	.12	N	<0.01	<0.01	SY1	
	SY1	57	4U	0	43.4	43.1	.14	N	<0.01	<0.01	SY2	
	SY2	43	19U	0	41.6	41.6	.13	N	<0.01	<0.01	ELG	
	LIN	10	1U	0	40.7	40.4	.18	N	0.60	1.1	SPIRR	
	ELG	37	8U	0	40.2	40.2	.15	N	1.7	3.2	SPIRR	
	SPIRR	22	7U	0	39.4	39.6	.17	38.5	3.9	11.8	E/S0	
	E/S0	17	3U	0	40.2	40.2	.22	48.6				
$\log L_{60\mu m}$	QSO	80	44U	0	45.8	45.2	.12	N	<0.01	<0.01	SY1	
	SY1	57	8U	0	44.2	44.1	.08	N	4.8	2.2	SY2	
	SY2	43	0	0	44.3	44.4	.10	N	0.01	<0.01	ELG	
	LIN	10	0	0	43.2	43.3	.22	N	4.2	5.2	SPIRR	
	ELG	37	0	0	43.6	43.6	.15	N	0.01	0.04	SPIRR	
	SPIRR	22	0	0	42.7	42.6	.15	N	73.4	92.8	E/S0	
	E/S0	17	0	0	42.6	42.5	.16	N	48.6			
$\log \frac{L_X}{L_{60\mu m}}$	QSO	67	35L	4U	-0.13	-0.27	.10	0.75	0.41	0.65	SY1	
	SY1	53	8L	4U	-0.67	-0.79	.13	N	<0.01	<0.01	SY2	A
	SY2	43	19U	0	-2.9	-2.8	.14	N	0.06	1.9	ELG	
	LIN	10	1U	0	-3.0	-2.8	.18	N	61.0	67.4	SPIRR	
	ELG	37	8U	0	-3.4	-3.4	.08	N	1.2	1.6	SPIRR	
	SPIRR	22	7U	0	-3.0	-3.0	.10	N	0.32	2.4	E/S0	
	E/S0	17	3U	0	-2.2	-2.4	.18	N				
$\alpha(25,60)$	QSO	36	9U	3L	-0.9	-0.8	.10	N	10.6	3.8	SY1	
	SY1	49	10U	4L	-1.1	-1.2	.12	N	5.2	4.3	SY2	
	SY2	43	2U	0	-1.4	-1.5	.12	N	0.05	0.9	ELG	
	LIN	10	0	0	-1.9	-2.2	.27	N	16.3	29.9	SPIRR	
	ELG	37	2U	0	-2.1	-2.1	.11	-4.3	0.43	0.42	SPIRR	
	SPIRR	22	5U	0	-2.6	-2.7	.20	N	5.2	24.5	E/S0	
	E/S0	17	5U	0	-2.2	-2.0	.25	-3.5				
$\alpha(60,100)$	QSO	29	11L	4U	-0.9	-0.8	.15	N	61.7	76.2	SY1	
	SY1	49	11L	1U	-0.9	-0.8	.14	N	2.6	16.7	SY2	
	SY2	43	4L	0	-0.5	-0.5	.10	N	3.8	17.5	ELG	
	LIN	10	0	0	-1.8	-2.0	.21	N	25.5	23.1	SPIRR	
	ELG	37	3L	0	-1.0	-0.9	.14	N	<0.01	0.01	SPIRR	
	SPIRR	22	0	0	-2.2	-2.2	.14	N	76.5	78.5	E/S0	
	E/S0	17	0	0	-2.3	-2.0	.15	N				
$\alpha(12,60)$	QSO	36	10U	3L	-0.9	-0.9	.07	N	2.0	1.2	SY1	
	SY1	49	22U	3L	-1.1	-1.2	.08	-2.0	0.9	0.9	SY2	
	SY2	43	18U	0	-1.5	-1.5	.13	N	1.4	17.2	ELG	
	LIN	10	0	0	-1.3	-1.4	.12	N	94.9	68.9	SPIRR	
	ELG	37	7U	0	-1.8	-1.8	.11	-2.5	0.7	15.4	SPIRR	
	SPIRR	22	4U	0	-1.4	-1.5	.13	-2.8	8.1	12.9	E/S0	
	E/S0	17	5U	0	-1.2	-1.1	.13	N				
Quasars: Radio-loud (RLQ) vs. Radio-quiet (RQQ)												
log z	RLQ	44	0	0	-0.2	-0.1	.06	N	<0.01	<0.01	RQQ	
	RQQ	39	0	0	-0.8	-0.6	.08	N	<0.01	<0.01	SY1	
$\log L_X$	RLQ	44	5U	0	45.8	45.7	.13	N	<0.01	<0.01	RQQ	
	RQQ	39	9U	0	44.7	44.4	.13	N	<0.01	<0.01	SY1	
$\log L_{60\mu m}$	RLQ	42	24U	0	45.5	45.7	.18	N	0.13	0.34	RQQ	
	RQQ	38	20U	0	44.7	44.8	.12	44.1	0.03	0.68	SY1	

Table 2 – *continued*

Parameter	Class	Sample Total	Limits	Deleted	Median	Mean	Error	Trunc?	Probability (%) Gehan	Logrank	Versus	Notes
$\log\frac{L_X}{L_{60\mu m}}$	RLQ	37	21L	2U	-0.14	-0.33	.09	0.2	67.6	80.5	RQQ	
	RLQ								0.9	3.7	SY1	
	RLQ								<0.01	<0.01	SY2	
	RQQ	30	14L	2U	-0.28	-0.29	.17	0.8	5.2	2.6	SY1	
	RQQ								<0.01	<0.01	SY2	
$\alpha(25,60)$	RLQ	18	6U	1L	-0.8	-0.9	.12	-1.6	74.8	84.6	RQQ	
	RLQ								27.0	21.1	SY1	
	RLQ								2.7	6.9	SY2	
	RQQ	18	3U	2L	-0.9	-0.8	.14	N	15.5	7.4	SY1	
	RQQ								0.6	1.4	SY2	
$\alpha(60,100)$	RLQ	12	5L	3U	-1.1	-1.0	.23	-0.1	43.8	42.7	RQQ	
	RLQ								84.2	81.6	SY1	
	RLQ								15.7	32.6	SY2	
	RQQ	16	6L	1U	-0.7	-0.7	.19	N	38.1	53.2	SY1	
	RQQ								71.1	78.0	SY2	
$\alpha(12,60)$	RLQ	18	7L	2U	-0.9	-0.9	.08	N	44.5	86.9	RQQ	
	RLQ								17.0	11.1	SY1	
	RLQ								0.2	0.5	SY2	
	RQQ	18	3U	1L	-0.9	-0.8	.11	N	1.5	2.3	SY1	
	RQQ								0.01	0.06	SY2	

(A) The predominant direction of limits differs in the two galaxy classes tested.

(IPAC) using the programs ADDSCAN and SCANPI. By combining all available scans of an object, sensitivity is increased by a factor of two or more over the PSC. Baseline fluxes in the equivalent apertures were subtracted, with the rms residual noise providing the noise estimate. We defined three flux-quality flags FQ for coadded data similar to those used in the PSC. The overall application of gain correction factors to ADDSCAN data ensures that fluxes (for true point sources) are consistent on average with those of the PSC (version 2.0). The fluxes derived from the PSC and those derived from coadded scans agree to within a few per cent. For galaxies of particularly large angular extent (≥ 8 arcmin blue-light isophotal diameter), we take fluxes from Rice *et al.* (1988), which are calibrated to PSC fluxes in the same way as our one-dimensional coadds. Coadded fluxes for two Seyfert 1 galaxies (NGC 4235 and NGC 4151) were taken from Edelson *et al.* (1987).

Infrared (IR) luminosities are derived assuming $L = \nu l_\nu$, where l_ν is the monochromatic luminosity in erg s^{-1} Hz^{-1}. We have chosen to use IR luminosities measured through the 60-μm band because this is where the data set has the greatest number of detections, and because the largest body of published *IRAS* luminosity functions are for 60 μm. The luminosity in the 60-μm band is

$$L = \frac{4\pi c^2}{H_0^2} \frac{z^2(1+z/2)^2}{(1+z)^{\alpha(25,100)+1}} \nu_{60} f_{60} ,$$

where $\alpha(25,100)$ is the spectral slope between 25 and 100 μm, and f_{60} is the 60-μm flux density in erg cm^{-2} s^{-1} Hz^{-1}. If either the 25-μm or the 100-μm flux is an upper limit, average values of $\alpha(25,100)$ calculated from the appropriate class of objects in our data set are used in the luminosity calculation. These are as follows: QSO, −0.9; Sy1, −1.2; Sy2, −1.6; ELG, −1.8; SPIRR, −1.5; and E/S0, −1.1. We have not made colour corrections to the IR fluxes. Corrections are not needed for galaxies with power-law infrared slopes of −1, and are generally small (<10 per cent) in all four of the *IRAS* wavebands for the typical spectral indices noted above.

3.2 X-ray data

The *Einstein* database is not from an all-sky survey, and has had no overall systematic processing akin to that of the PSC. The X-ray data we use are consequently more heterogeneous than the infrared data. Nevertheless, virtually all the X-ray measurements were taken with the Imaging Proportional Counter (IPC) aboard the *Einstein Observatory*, although a few were obtained with the High Resolution Imager (HRI). Broadband X-ray flux estimates for the IPC are relatively insensitive to the choice of spectral parameters, enabling us to use X-ray data published by other workers.

For 16 galaxies, some of which were targets of *Einstein* observations, we did not find published X-ray data, and made our own measurements at the Harvard Smithsonian Center for Astrophysics (CfA). Our methods are described by Anderson & Margon (1987). Galaxies with previously unpublished X-ray data include, in order of increasing right ascension (T = target of *Einstein* observation): MKN 334(T), NGC 513, *IRAS* 01217+0122, MKN 359, MKN 1034 = AKN81(T), NGC 1052(T), NGC 1685(T), NGC 3281, *IRAS* 10502-1018, NGC 4378(T), MKN 268(T), PG 1345(T), 3C 327(T), IC 4870(T), MKN 896, PK 2048(T). We discovered that the far-infrared luminous galaxies *IRAS* 01217+0122 and *IRAS* 10502−1843 (Heckman, Armus & Miley 1987) had been included serendipitously in *Einstein* exposures. Based on optical line ratios published by Heckman *et al.* (1987) we tentatively classify *IRAS* 01217+0122 as a Sy2. Due to insufficient data for *IRAS* 10502−1843,

classification is less certain, but the object also appears to fall with Sy2 on the [N II]/Hα versus [O I]/Hα and the IR colour–colour diagrams, so we have classified it as such in this paper.

Since the signal-to-noise ratio is often low, flux estimates for AGN usually assume some canonical X-ray spectrum. The X-ray spectra of AGN are commonly fitted by a power law of spectral index α_X. For galaxies without active nuclei (both spirals and ellipticals), thermal bremsstrahlung spectra rather than power laws provide a better description of the data (see Fabbiano 1989 for a comprehensive review).

For much of our data set, X-ray luminosities were originally derived between 0.5 and 4.5 keV (e.g. Tananbaum *et al.* 1986; Green *et al.* 1989), and we have chosen to convert other published X-ray luminosities to this bandpass, when necessary. To obtain a conversion factor we have integrated the flux density f_ν of the appropriate spectral model (thermal or power law) over the standard bandpass and divided by the same integral over the published bandpass. Complicated assumptions involving soft X-ray absorption and K-corrections are required to convert from one spectral model to another, so we retain the models (or spectral fit parameters) preferred by the authors whose data we incorporate. X-ray luminosities in Table 1 are in the rest frame of the source, corrected for Galactic N_H, and converted to a 0.5–4.5 keV bandpass. For the $\lesssim 40$ per cent of the X-ray luminosities requiring such conversion, the mean bandpass conversion factor is 0.83 ± 0.24, with extreme values of 0.2 and 1.4.

For emission-line (i.e. starburst and H II-region), spiral, and irregular galaxies, a thermal X-ray spectrum is most often assumed, consistent with spectral fits to spiral and emission-line galaxies (Fabbiano & Trinchieri 1987). For the great majority of such objects, X-ray luminosities were published in the 0.5–3 keV band assuming a 10-keV thermal model (Long & Van Speybroeck 1983). These values are very similar to those one would derive in the standard 0.5–4.5 keV range by assuming a more appropriate temperature near 4 keV. Since this latter temperature is in greater accord with actual spectral fits, no bandpass conversions are required. For normal elliptical and S0 galaxies, fits have shown thermal spectra of 1 keV to be more appropriate (Forman, Jones & Tucker 1985), and the X-ray data we include for this class of galaxies (from Canizares, Fabbiano & Trinchieri 1987) were originally derived in our chosen bandpass with such a 1-keV thermal model.

When available, published fluxes obtained from X-ray spectral fits were used, since they provide the most reliable estimates of true flux. The power-law fits by Wilkes & Elvis (1987) list 0.3–3.5 keV fluxes, while Kruper, Urry & Canizares (1990) adopt 0.2–4 keV. Where multiple observations are published, we use the unabsorbed X-ray luminosity with the lowest value of χ^2.

4 STATISTICAL RESULTS

In this section we discuss first the univariate, and then the bivariate statistical results. We employ, with some minor modification, the survival analysis software package generously provided to us by T. Isobe & E. Feigelson. Our application of these methods, and the results in Tables 2–4, are explained in the Appendix.

4.1 Univariate results

We use non-parametric Kaplan–Meier maximum likelihood tests to provide means and medians of the distributions of a given parameter. Distributions for two different samples (e.g. two classes of galaxy) may also be quantitatively compared. Since our data set is heterogeneous in origin, we prefer to emphasize discussion of galaxy flux ratios and spectral properties which suffer less from selection effects than do luminosities.

There is a trend of steadily decreasing mean $L_X/L_{60\,\mu m}$ ratio from QSO through Seyfert through SPIRR to ELG classes. The X-ray luminosity of QSO and Sy1 is 10–50 per cent of their 60-μm luminosity. We find that QSO and Sy1 are not significantly different in $L_X/L_{60\,\mu m}$, and both are distinguished from any of the other classes by their relatively much stronger X-ray emission. The next two classes of galaxy descending in value of $L_X/L_{60\,\mu m}$ are the E/S0 and Sy2, where this ratio is of order 0.5 per cent for each. That these two types of galaxies, the latter active and dusty, and the former inactive and relatively dust-free, have similar X-ray to IR ratios exposes the primary factors determining the ratio: activity raises $L_X/L_{60\,\mu m}$ by increasing the X-ray emission, while the gas associated with dusty regions decreases it by simultaneously absorbing the soft X-rays and boosting the IR radiation. We should thus expect the lowest mean value of $L_X/L_{60\,\mu m}$ to come from the class having a propitious combination of the least non-thermal (i.e. non-stellar) activity and the most dust. Consistent with the dust-enshrouded regions of intense star formation often associated with them, the lowest mean of $\log(L_X/L_{60\,\mu m})$ by far is that of the ELG at -3.4.

A primary finding of this study is that the ratio $L_X/L_{60\,\mu m}$ provides an excellent diagnostic of optical broad-line emission. A histogram of $\log(L_X/L_{60\,\mu m})$ values for galaxies in our data set (Fig. 1) reveals a strong bimodality, where the broad

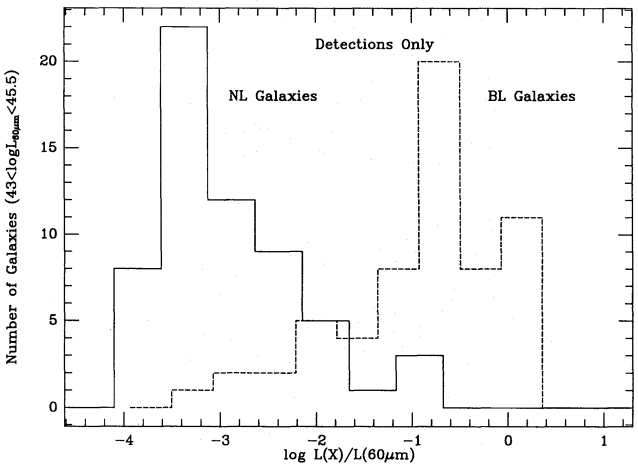

Figure 1. A histogram of the ratio of $\log L_X/L_{60\,\mu m}$ for galaxies with narrow and broad optical emission lines, respectively. Only galaxies in the region of strong overlap between the NL and BL branches, where $43 < \log L_{60\,\mu m} < 45.5$, are plotted. This restriction assures that a luminosity effect is not responsible for the bimodality, which in any case is equally strong when all galaxies are included. Although the figure shows only galaxies detected by both *IRAS* and *Einstein*, the preponderant directions of limits in this ratio for BL and NL galaxies only increase their separation (see Section 4.1).

optical emission-line objects (Sy1 and QSO) are separated from all other types of galaxy here represented. Since the full IR/X sample covers a large range of luminosities, we initially suspected that the difference in the ratio might be a luminosity effect, since narrow emission-line (NL) and broad emission-line (BL) galaxies span substantially different ranges of luminosity. We have thus only counted galaxies in the region of strong overlap between the two branches, where $43 < \log L_{60\,\mu m} < 45.5$. Although Fig. 1 shows only galaxies detected by both *IRAS* and *Einstein*, the directions of limits in this ratio for BL and NL galaxies would only increase their separation. From the figure, a galaxy with a log ratio of far-IR to soft X-ray flux greater than about -2 has a very high probability of being either a Sy1 or a QSO. This criterion will be valuable for finding broad emission-line galaxies from comparisons of IR and X-ray surveys. A sensitive, all-sky survey like *ROSAT* is particularly well-suited to such a search in conjunction with *IRAS* or other, future far-IR surveys.

4.2 Bivariate results

We consider correlations between two variables to be significant if the probability P of their independence is less than 2.0 per cent using non-parametric rank correlation tests (see Appendix). The upper right half of Table 3 displays the strength of correlations ('W' for weak, 'S' for strong) for the entire IR/X ensemble of galaxies between parameters listed across the top and left-hand sides. Symbols in parentheses indicate that, due to selection effects, other samples may be better suited to analysis of the variables involved.

The results of regression analyses for correlations shown to be strong are in Table 4. In deriving the best-fitting linear regression, we use a two-dimensional Kaplan–Meier test (Schmitt 1985) that allows censoring (of a single type) in both variables (see Appendix).

4.2.1 X-ray versus 60-μm luminosity

The plot of $L_{60\,\mu m}$ against X-ray luminosity (Fig. 2) shows a very strong correlation, with a marked offset in the trend at $\log L_{60\,\mu m} \approx 44.5$ or $\log L_X \approx 43.0$. Although there is some mixing, the offset creates two well-separated branches. On one branch are located the broad optical emission-line objects (Sy1 and QSO), while the other is populated almost exclusively by narrow emission-line objects and normal galaxies. The BL branch has nearly the same slope as the NL branch, but with a strong offset toward higher X-ray luminosities.

We are confident that both the correlation and the shift between these two lines in the $L_{60\,\mu m}$ versus L_X plane are real. We have plotted f_X versus $f_{60\,\mu m}$ and found a clear separation between NL and BL groups as well as strong ($P < 1$ per cent) correlations in each group separately. Correlations within each branch also persist for separate galaxy types in a flux–flux plot.

The separation of the NL and BL lines suggests a division in predominance of stellar and nuclear non-thermal processes between the two trends. The most important mixing between branches occurs in the Seyfert classes, consistent with reports of significant starburst activity in both Sy1 and Sy2 galaxies, and with hints of broad line emission in the reflected polarized light of Sy2 (Antonucci & Miller 1985). A composite in the infrared of thermal and non-thermal emission processes in Seyferts has been suggested in a number of studies (e.g. Hunt 1991; Wilson 1988; Ward *et al.* 1987). Arguments that AGN emission-line spectra (including broad permitted lines and variability) can be reproduced by violent star-formation processes in a high-metallicity nuclear environment (e.g. Terlevich & Melnick 1985) are not supported by the sharp discontinuity between the branches in Fig. 2. Without the addition of some new (e.g. non-thermal) mechanism, a simple scaling-up of nuclear starburst regions toward greater luminosities would not be expected to cause the sudden increase in the ratio $L_X/L_{60\,\mu m}$ seen at about $\log L_X \approx 43.0$.

From Table 4, if we assume that the intrinsic dependence is of L_X upon $L_{60\,\mu m}$, the best fit to the relation $L_X \propto L_{60\,\mu m}^{\alpha}$ for all galaxies is $\alpha = 1.3 \pm 0.07$. This slope shows the increase in X-ray relative to IR luminosity as nuclear sources predominate, but is certainly not representative of the distinct physical processes intrinsic to the broad- and narrow-line branches individually. For these branches respectively, the slopes 0.82 ± 0.08 and 0.78 ± 0.07 demonstrate a *decrease* in the X-ray to IR ratio with increasing luminosity. The non-

Table 3. Correlation test results.

	$\log L_{60\mu m}$	$\log L_X$	$\log \frac{L_X}{L_{60\mu m}}$	$\alpha(25,60)$	$\alpha(60,100)$	$\alpha(12,60)$	log z
$\log L_{60\mu m}$	*	S	W	(S)	(S)	(W)	(S)
$\log L_X$	S/S	*	S	S	S	S	(S)
$\log \frac{L_X}{L_{60\mu m}}$	.	S/S	*	S	W	S	S
$\alpha(25,60)$	.	S/W	S/S	*	(W)	(S)	(S)
$\alpha(60,100)$	.	W/S	.	.	*	(W)	(S)
$\alpha(12,60)$	.	S/W	S/W	.	.	*	(W)
log z	.	.	S/W	.	.	.	*

All Galaxies

Broad/narrow optical emission line galaxies

W – Weak correlation ($P > 2$ per cent for any test). S – Strong correlation ($P < 2$ per cent for all tests). Parentheses indicate that other samples may be better suited to analysis of a correlation between these variables.

Table 4. Bivariate results: correlation and regression tests.

Parameters X	Parameters Y	Class	Test	N_{total}	Limits X low	Limits X up	Limits Y low	Limits Y up	Both	Prob. (%)	Slope	Intercept	Limits Changed X	Limits Changed Y	Limits Changed Both
$\log L_{60\mu m}$	$\log L_X$	ALL	BHK/2KM	266	0	52	0	55	9	<.01	1.3 ±.07	−14.3 ±2.8	3	5	0
$\log L_X$	$\log L_{60\mu m}$	ALL	2KM	266	0	55	0	52	9		0.41 ±.02	26.7 ±1.0	6	9	0
			mean y(x)								1.73	−33.8			
		BL	BHK/2KM	137	0	52	0	17	9	<.01	0.82 ±.08	7.3 ±3.8	9	3	0
		BL	2KM	137	0	17	0	52	9		0.49 ±.07	23.0 ±3.2	3	9	0
			mean y(x)								1.26	-12.4			
		QSO	BHK/2KM	80	0	44	0	13	9	<.01	0.62 ±.09	17.0 ±3.9	11	2	0
		QSO	2KM	80	0	13	0	44	9		0.68 ±.11	14.5 ±5.0	2	11	0
			mean y(x)								0.95	1.8			
		RLQ	BHK/2KM	41	0	23	0	4	2	.01	0.63 ±.09	16.9 ±3.9	6	1	0
		RLQ	2KM	41	0	4	0	23	2		0.77 ±.17	10.9 ±7.5	1	6	0
			mean y(x)								0.91	3.1			
		NL	BHK/2KM	129	0	0	0	36	0	<.01	0.78 ±.07	6.8 ±3.1	0	2	0
		NL	2KM	129	0	36	0	0	0		0.77 ±.07	12.3 ±2.9	4	0	0
			mean y(x)								1.01	−3.1			
		ELG	BHK/2KM	37	0	0	0	8	0	<.01	0.77 ±.12	6.7 ±5.2	0	0	0
		ELG	2KM	37	0	8	0	0	0		0.94 ±.12	5.6 ±4.7	0	0	0
			mean y(x)								0.91	0.83			
		SPIRR	BHK/2KM	22	0	0	0	7	0	.03	0.83 ±.13	4.3 ±5.3	0	1	0
		SPIRR	2KM	22	0	7	0	0	0		0.78 ±.15	11.7 ±6.1	1	0	0
			mean y(x)								1.0	−4.3			
$\log L_X$	$\log \frac{L_X}{L_{60\mu m}}$	ALL	BHK	257	0	46	43	46	46	<.01					
		ALL	2KM	214	0	46	0	46	46		0.50 ±.03	−23.0 ±1.1	0	0	0
$\log \frac{L_X}{L_{60\mu m}}$	$\log L_X$	ALL	2KM	214	43	35	0	35	35		1.31 ±.07	44.9 ±0.2	7	0	2
			mean y(x)								0.62	−28.3			
		BL	BHK	128	0	8	43	8	8	<.01					
		BL	2KM	120	0	0	43	0	0		0.33 ±.07	−15.3 ±2.9	0	0	0
		BL	2KM	120	43	8	0	8	8		0.87 ±.10	44.8 ±0.2	0	0	1
			mean y(x)								0.66	−30.1			
		NL	BHK	129	0	38	0	38	38	<.01					
		NL	2KM	129	0	38	0	38	38		0.28 ±.07	−14.1 ±2.8	0	0	1
		NL	2KM	129	0	38	0	38	38		0.84 ±.18	42.8 ±0.5	0	0	1
			mean y(x)								0.64	−28.9			
log z	$\log \frac{L_X}{L_{60\mu m}}$	ALL	EM	257	0	0	43	46	0		0.79 ±.06	−0.7 ±.11	0	0	0
$\log \frac{L_X}{L_{60\mu m}}$	log z	ALL	BHK/2KM	214	35	43	0	0	0	<.01	0.32 ±.04	−1.0 ±.09	7	0	0
			mean y(x)								1.44	0.4			
		BL	EM	128	0	0	43	8	0		0.62 ±.15	0.1 ±.20	0	0	0
		BL	BHK/2KM	128	43	8	0	0	0	.05	0.18 ±.06	−0.9 ±.08	0	4	0
			mean y(x)								1.21	0.2			
$\log L_X$	$\alpha(25,60)$	ALL	BHK	221	0	47	7	33	12	<.01					
		ALL	2KM	214	0	46	0	33	11		0.26 ±.03	−12.5 ±1.3	3	5	1
$\alpha(25,60)$	$\log L_X$	ALL	2KM	214	0	33	0	46	11		1.17 ±.10	43.7 ±0.2	10	6	0
			mean y(x)								0.52	−23.4			
		BL	BHK	92	7	19	0	9	4	.25					
		BL	2KM	85	0	8	0	19	3		0.15 ±.06	−7.6 ±2.7	3	3	0
		BL	2KM	85	7	17	0	9	4		0.64 ±.23	44.4 ±0.2	6	3	0
			mean y(x)								0.65	−29.4			
$\log L_X$	$\alpha(60,100)$	ALL	BHK	211	0	46	29	5	11	.21					
			2KM	206	0	46	29	0	11		0.13 ±.05	−6.5 ±2.0	4	0	0
$\alpha(60,100)$	$\log L_X$	ALL	2KM	211	29	5	0	46	11		0.11 ±.19	41.8 ±0.3	7	5	1
			mean y(x)								1.0	−43.6			
		NL	BHK/2KM	129	7	0	0	36	6	<.01	0.44 ±.12	41.0 ±0.2	0	3	2
		NL	2KM	129	0	36	7	0	6		0.37 ±.10	−16.5 ±4.1	3	0	0
			mean y(x)								1.0	42.0			

Table 4 – *continued*

Parameters X	Parameters Y	Class	Test	N_{total}	Limits X low	Limits X up	Limits Y low	Limits Y up	Both	Prob. (%)	Slope	Intercept	Limits Changed X	Limits Changed Y	Limits Changed Both
$\log\frac{L_X}{L_{60\mu m}}$	$\alpha(25,60)$	ALL	BHK	220	6	46	6	33	17	<.01					
		ALL	2KM	214	0	46	0	33	11		0.43 ±.04	−0.7 ±0.1	6	5	0
$\alpha(25,60)$	$\log\frac{L_X}{L_{60\mu m}}$	ALL	2KM	221	0	33	0	46	11		0.68 ±.09	−1.1 ±0.2	5	6	0
			mean y(x)								0.83	0.2			
		BL	BHK/2KM	91	0	8	0	19	3	<.01	0.37 ±.08	−0.63 ±0.1	3	2	0
		BL	2KM	85	0	19	0	8	3		0.77 ±.12	−0.26 ±0.2	2	2	0
			mean y(x)								0.73	−0.25			
		NL	BHK/2KM	129	0	36	0	14	7	0.58	0.22 ±.15	−1.4 ±0.5	0	4	0
		NL	2KM	129	0	14	0	36	7		0.08 ±.07	−2.8 ±0.2	4	0	0
			mean y(x)								1.14	1.4			
$\log L_X$	$\alpha(12,60)$	ALL	BHK	220	0	47	6	66	27	<.01					
			BHK	214	0	47	0	66	26		0.13 ±.02	−6.9 ±0.8	6	5	1
$\alpha(12,60)$	$\log L_X$	ALL	2KM	214	6	65	0	46	26		1.48 ±.21	43.8 ±0.3	7	5	1
			mean y(x)								0.38	−17.2			
		BL	BHK	90	0	9	6	31	6	0.8					
			2KM	84	0	9	6	29	6		0.10 ±.04	−5.4 ±1.6	3	0	2
		BL	2KM	84	6	29	0	9	6		1.0 ±.4	44.9 ±0.4	3	2	2
			mean y(x)								0.47	21.8			
$\log\frac{L_X}{L_{60\mu m}}$	$\alpha(12,60)$	ALL	BHK	219	5	46	5	66	31	<.01					
			2KM	214	0	46	0	66	26		0.31 ±.03	−0.7 ±0.06	3	7	0
$\alpha(12,60)$	$\log\frac{L_X}{L_{60\mu m}}$	ALL	2KM	214	0	66	0	46	26		1.28 ±.12	−0.4 ±0.2	7	3	0
			mean y(x)								0.52	−0.2			
		BL	BHK	90	5	8	5	32	10	<.01					
			2KM	85	0	8	0	32	5		0.29 ±.04	−0.7 ±0.1	3	1	1
		BL	2KM	85	0	32	0	8	5		1.6 ±.19	0.6 ±0.2	1	3	1
			mean y(x)								0.45	−0.5			

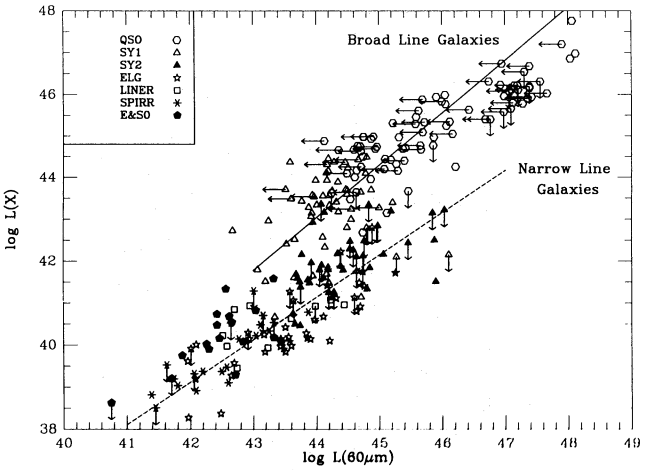

Figure 2. Plot of $\log L_X$ versus $\log L_{60\mu m}$ for all galaxies. The luminosities L_X and $L_{60\mu m}$ are in units of erg s^{-1}. Symbols for the different galaxy classes are shown in the upper left, and their acronyms are described in Section 2. Mean regression lines are shown separately for broad (BL) and narrow (NL) emission-line galaxies. The mean regression is defined as the bisector of the two best-fitting lines found by regressing $y(x)$ and then $x(y)$. Upper limits are indicated with arrows. (See Section 4.2.1).

linearity is not due to a distance or aperture effect: the plot of $L_X/L_{60\mu m}$ versus $\log z$ again shows a much weaker correlation for BL, and no correlation for NL galaxies. A similar non-linear relationship has been seen with the near-infrared in radio-quiet quasars alone (Worrall 1987; Kriss 1988).

It is revealing to subdivide the data set further and examine the luminosity correlations within individual classes of galaxy. Seyfert 1 and 2 galaxies are the only classes showing little or no correlation ($P=11$ and 32 per cent respectively). For E/S0, the strength of the correlation is nearly as weak as in Sy2, but this may be at least partially attributed to the small sample size (17 objects). SPIRR and ELG each show strong correlations with slopes 0.83 ± 0.13 and 0.77 ± 0.12 respectively, closer to linear than the mean slope exhibited by QSO (0.62 ± 0.09). ELG and SPIRR classes show strong correlations due to a predominance of stellar activity, while the QSO correlation illustrates the strong intrinsic non-thermal component. We believe that, since stellar and non-thermal nuclear components – whose respective ratios $L_X/L_{60\mu m}$ differ significantly – are strongly mixed in Seyfert 1 and 2 galaxies, the correlation intrinsic to each component alone is lost. This interpretation is reinforced when we divide the QSO into radio-quiet (RQQ) and radio-loud (RLQ) subclasses for a similar analysis. Only the RLQ show a significant correlation (of slope 0.63 ± 0.09). Unlike for some RLQ, the IR radiation of the RQQ can be modelled with purely thermal components (Lawrence *et al.* 1991; Sanders *et al.* 1989). The RQQ should then be grouped with Sy1, as is indicated by their continuity in other parameters also. The complexity of potential contributors to both the IR and X-ray emission from galaxies assures that there is a

variety of ways in which this non-linearity could be explained.

We urge caution in interpreting the physical significance of non-linear regressions that have assumed *a priori* some intrinsic dependence. Most previous studies involving censored data have emphasized regressions where upper limits are in the dependent variable alone. Regressions performed on either axis alone are frequently non-linear. For instance, if $L_{60\,\mu m}$ for all quasars is regressed on L_X, the resulting best-fit yields a slope (0.68 ± 0.11) identical within the errors to that obtained by regressing L_X on $L_{60\,\mu m}$ (0.62 ± 0.09). The slope of the line which bisects these alternate regression lines is generally consistent with unity (see Table 4).

4.2.2 *X-ray versus 12-, 25-, and 100-μm luminosities*

We have examined plots and correlations of L_X versus L_{IR} for the *IRAS* 12-, 25-, and 100-μm bands. The latter two correlations resemble very closely the L_X versus $L_{60\,\mu m}$ relation of Fig. 2. The plot of X-ray luminosity with $L_{12\,\mu m}$ (Fig. 3) is considerably better defined, yet, just as in the $L_{60\,\mu m}$ plot, Seyferts still show no significant correlation.

Spignolio & Malkan (1989) suggest that AGN (QSO, Sy1 and Sy2) energy distributions can be described by a one-parameter family: an intrinsically blue quasar continuum modified by the presence of varying quantities of dust. Since the dust absorbs short-wavelength continuum and re-emits in the infrared, they argue that there must be a 'pivot' wavelength where the absorption and re-emission balance, resulting in a very small net modification of the continuum. The 'pivot' wavelength (near 12 μm) should be the best estimator of L_{bol}, even in the presence of varying quantities of absorbing dust. For the AGN in our data set, since L_X best represents the intrinsic nuclear non-thermal luminosity, such a model may explain the tighter correlation observed between L_X and $L_{12\,\mu m}$ compared to that at $L_{60\,\mu m}$.

4.2.3 *X-ray luminosity versus IRAS colours*

When the *IRAS* warmth criterion mentioned in Section 2 $[\alpha(25,60) \geq -1.5]$ is imposed on Sy1 or Sy2, the resulting subsets have higher mean L_X and higher mean ratio $L_X/L_{60\,\mu m}$. That is, warm Seyferts tend to be more powerful X-ray emitters. This trend is illustrated by the strong positive correlation between $\alpha(25,60)$ and L_X (see Fig. 4).

All three *IRAS* colours $\alpha(25,60)$, $\alpha(60,100)$, and $\alpha(12,60)$ correlate strongly with L_X over the full data set. When restricted to BL galaxies, only the correlation with $\alpha(60,100)$ becomes weak. This colour is a measure of the relative quantity of cool dust in the galaxy, a quantity which is expected to correlate with the strength and extent of star-forming regions, but which is a poor predictor of nuclear luminosities. In concordance with these expectations, only this same correlation $[\alpha(60,100)$ with $L_X]$ remains strong when restricted to NL galaxies (see Table 3). ELG and SPIRR types are X-ray bright by virtue of Population I type sources, for example massive X-ray binaries. Apparently, the number of these sources does not determine the dust temperatures [as measured by $\alpha(25,60)$] in the star-formation regions that harbour them.

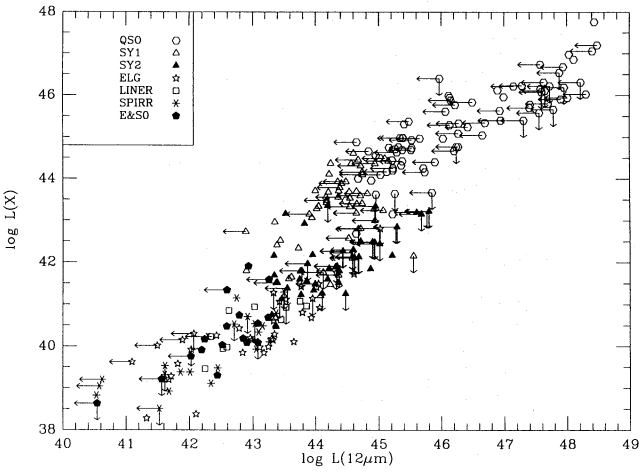

Figure 3. Plot of $\log L_X$ versus $\log L_{12\,\mu m}$ for all galaxies. Symbols and units are as described in Fig. 2. The correlation of X-ray with 12-μm luminosity is even stronger than the correlation illustrated in Fig. 2 (see Section 4.2.1).

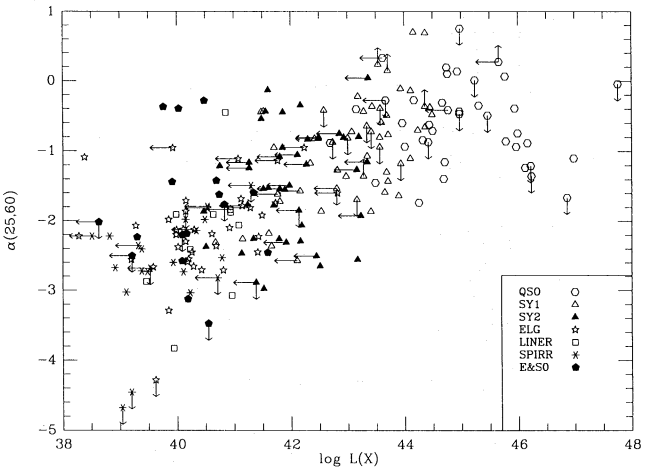

Figure 4. Plot of $\alpha(25, 60)$ versus $\log L_X$ for all galaxies. Symbols and units are as described in Fig. 2. Objects with warmer IR spectra [larger $\alpha(25, 60)$] are known to exhibit higher levels of nuclear activity, and are seen here to correspond to higher X-ray luminosities (see the discussion in Section 4.2.3).

Edelson *et al.* (1987) have investigated the infrared extent of Seyfert galaxies by comparing narrow-beam ground-based 10.6-μm flux and *IRAS* 12-μm flux. They find that larger values of the infrared spectral slope $\alpha(12,60)$ indicate more compact sources. The strong correlation we find of $\alpha(12,60)$ with L_X in BL but not NL galaxies probably highlights the predominance of compact nuclear emission in BL galaxies, and of extended Population I sources in NL galaxies.

5 PROPERTIES OF SELECTED GALAXY CLASSES

5.1 Quasars

We find similar mean $\log L_X/L_{60\,\mu m}$ for RLQ and RQQ, so that similar ratios are characteristic of the emission mechanisms in both types of quasar. There is no significant difference between RLQ and RQQ in our data set for all

distance-independent (e.g. colour or spectral) parameter distributions compared in univariate tests.

To compare our far-infrared results to published (near-infrared) work, we must use regressions performed only in one direction, assuming that the primary dependence is of X-rays on the near-infrared ($L_X \propto L_{\rm NIR}$). We find for BL galaxies (Sy1 + RQQ + RLQ) a non-linearity ($L_X \propto L_{60\,\mu\rm m}^{0.82\pm0.08}$) similar to those of the RQQ samples of Kriss (1988) and Worrall (1987). However, the correlation between L_X and $L_{60\,\mu\rm m}$ is not significant, either for radio-quiet quasars ($P > 54$ per cent) or Sy1 ($P = 32$ per cent). Similarly, no correlation has been seen between 2-keV and 3-μm luminosities in PG quasars (Sanders *et al.* 1989), or in Seyfert 1s (McAlary & Rieke 1988).

We do find a strong correlation for radio-loud quasars ($P = 0.01$ per cent), as might be expected if both wavebands in RLQ are dominated by a non-thermal source. For RLQ, we find the best-fitting regressions to be $L_X \propto L_{60\,\mu\rm m}^{0.62\pm0.09}$. Our first suspicion was that luminosity correlations might be strongly influenced by selection effects: the X-ray-detected RLQ cover a greater range in redshift than the RQQ, but this is not the case. If, invoking their continuity in properties, we combine RQQ and Sy1, a very large redshift range is sampled, and still no significant correlation between X-ray and IR luminosities appears. The RLQ correlation is likewise not a selection effect, since it persists on a flux–flux plot.

Wilkes & Elvis (1987) found that only RQQ have the steep X-ray slopes needed to join the X-rays to the near-infrared ($\alpha \approx -1$). This implies an intrinsic connection via a non-thermal central source between the two bands in RQQ, but not for RLQ. This appears to be contradicted by our findings that only RLQ show a strong correlation between X-rays and far-infrared luminosity unless both (a) a true RQQ correlation is washed out by stellar contamination in the far-infrared and (b) the RLQ correlation is spurious or not intrinsic, e.g. a redshift effect. We have ruled out the latter possibility. Also, with or without coordinated variability in the X-rays, RQQ do not display short-term IR variability.

Since a coincidence of the mean ratio $L_X/L_{60\,\mu\rm m}$ in thermal and non-thermal emission mechanisms seems improbable, the similarity of this ratio in RLQ and RQQ suggests similar emission mechanisms. This is puzzling in light of our finding that IR and X-ray luminosities correlate only in RLQ. If we assume either that RLQ reside in elliptical galaxies or have strong non-thermal emission, or both, it is not possible to resolve the puzzle of the similarity of the ratio $L_X/L_{60\,\mu\rm m}$ in RLQ and RQQ. The ratio appears to be highest for a pure non-thermal source, and we have shown (Table 2) that it also is higher for normal elliptical galaxies than for spiral or starburst-region galaxies. Either trend would conspire to give RLQ a significantly higher ratio, which is not seen.

5.2 Seyfert galaxies

Among colour or spectral parameters, Sy1 and RQQ show no statistically significant differences. The RQQ always form a continuum of properties with Sy1 on all X-ray and/or IR plots, while the RLQ are often clearly offset from the trends.

Sy1 and Sy2 are strongly distinguished only by $\alpha(12, 60)$ or the ratio $L_X/L_{60\,\mu\rm m}$, highlighting similar disc emission with a much stronger nuclear component observed in Sy1.

5.3. Emission-line galaxies

The high IR luminosities of ELG reveal the prodigious quantity of dust and gas amid powerful radiation from large star-forming regions. The Population I sources of X-ray radiation (OB stars, supernovae, and massive X-ray binaries) do not quite keep pace, and the slope of the $L_X(L_{60\,\mu\rm m})$ relation for ELG is 0.77 ± 0.12. The non-linearity of this relationship deserves explanation before we attempt explanations of non-linearity in AGN. As mentioned previously, Fabbiano *et al.* (1988) also found an exponent significantly different from unity for spiral galaxies and interpreted it as evidence that large obscured starburst regions are more common in more luminous galaxies.

5.4 Normal galaxies

For SPIRR, we find $L_X \propto L_{60\,\mu\rm m}^{0.83\pm0.13}$, the closest to linear of any of the galaxy classes within which a correlation is significant. The same correlation is stronger yet flatter for ELG. We can think of the SPIRR, where both disc and bulge may contribute substantially, as intermediate to the ELG (strong Population I contribution) and E/S0 (strong Population II). Possibly due to the small sample size (17 galaxies), there is a weaker correlation between L_X and $L_{60\,\mu\rm m}$ for E/S0 ($P \approx 4$ per cent), but regression yields a slope of 0.93 ± 0.28. Fabbiano *et al.* (1988) find that correlations between all luminosities (H or B band, far-infrared, radio and X-rays) are stronger in late-type spirals than in early-type. We speculate that the respective slopes are evidence that bulge/elliptical components foster more nearly linear relationships between X-ray and IR emission than do disc/spiral components.

6 CONTRIBUTION OF GALAXIES TO THE X-RAY BACKGROUND

A number of groups (e.g. Weedman 1991; Danese *et al.* 1987; Persic *et al.* 1989; Griffiths & Padovani 1990; Lonsdale & Harmon 1991) have recently made estimates of the possible contribution of active star-forming galaxies to the cosmic diffuse X-ray background radiation (hereafter, XRB). One motivation for such studies has been the work of Hamilton & Helfand (1987) (hereafter, HH) and Barcons & Fabian (1989) who find a high degree of isotropy on scales of a few square arcminutes in the soft XRB at energies of a few keV. The isotropy they find suggests that, if discrete X-ray sources are to dominate the soft XRB, they must have a very high surface density (e.g. of order 5000 deg^{-2}). HH and others argue that QSO are unlikely to be the dominant contributors to the XRB because they are not sufficiently numerous to satisfy the stringent X-ray isotropy constraints. Galaxies, on the other hand, do have high space/surface densities and at least certain classes (e.g. AGN and the more numerous star-forming galaxies) are known to emit strongly in X-rays. Thus X-ray emitting galaxies offer an attractive alternate discrete-source explanation for the origin of the XRB, one that might account for the observed isotropy, intensity, and perhaps even the spectrum of the XRB (e.g. see Griffiths & Padovani 1990; hereafter GP, for a detailed discussion).

Galaxies detected by *IRAS* have been found to include many star-forming and active galaxies, and the *IRAS* database has provided excellent information of the 60-μm luminosity function (hereafter LF) of galaxies (e.g. Saunders *et al.* 1990, and references therein). Our analysis of the empirical relationship between L_X and $L_{60\,\mu m}$ for various classes of galaxies allows us to convert such 60-μm *IRAS* LFs into estimates of the X-ray LF of IR-emitting galaxies, and thereby estimate the contribution of IR-emitting galaxies to the XRB.

Our approach closely parallels that of GP, but our determination of the empirical relationship between L_X and $L_{60\,\mu m}$ for IR-emitting galaxies includes more than four times as many galaxies and encompasses a range in 60-μm luminosity about 2.5 orders of magnitude greater than the sample used by GP. Further, we use a recent determination of the 60-μm LF of galaxies (due to Saunders *et al.* 1990) which differs considerably from the 60-μm LFs used by GP. The Saunders *et al.* LFs are much lower in normalization, and flatter at the faint end. Saunders *et al.* (1990) argue that the previous determinations of the 60-μm LF (e.g. those reported by Lawrence *et al.* 1986; Soifer *et al.* 1987; Sanders *et al.* 1988, etc.) are biased by galaxy clustering, and do not properly correct for an overdensity of low (60 μm) luminosity galaxies in the local supercluster. Finally, we also include quantitative information on the rate of evolution of the 60-μm LF.

6.1 Relation between L_X and $L_{60\,\mu m}$ for 'narrow-line' (non-Seyfert) IR galaxies

As discussed in Section 4.2.1 there appears to be a relatively simple relation between L_X and $L_{60\,\mu m}$ which may apply to a wide variety of *IRAS*-detected galaxy classes and over a wide range in 60-μm luminosity. In particular, the branch labelled 'NL' in Fig. 2 includes spiral and irregular, elliptical and S0, starburst, LINER, and Sy2 galaxies (but *not* Sy1 and QSO). This 'narrow-line' class includes 129 galaxies detected at 60 μm by *IRAS*, most also detected in X-rays (there are 36 X-ray non-detections among this group). The Sy2, however, appear to occupy a transition region between narrow- and broad-line branches. We are primarily interested in estimating the XRB contribution from more typical IR-emitting galaxies, and the space densities of Sy2 are quite small compared with other classes of galaxies at modest IR luminosities. For most of this section, we will thus also exclude the (43) Sy2 from consideration. The linear regression relation, incorporating X-ray non-detections and with L_X as the dependent variable, for such narrow-line galaxies, *excluding* Sy2, is

$$\log L_X = b + a \log L_{60\,\mu m} \qquad (1)$$

with $b = 12.4 \pm 3.1$ and $a = 0.64 \pm 0.07$. For our XRB estimate, we will assume that equation (1) applies for all IR-emitting galaxies with 60-μm luminosity in this range. A similar unity in the L_X to $L_{60\,\mu m}$ relationship for several *IRAS*-detected galaxy types has also been suggested by GP.

6.2 Estimating the contribution of IR galaxies to the XRB

We use the 60-μm galaxy LFs determined by Saunders *et al.* (1990) for *IRAS* galaxies. Additionally, those authors provide a quantitative, empirical estimate for the rate of evolution of the 60-μm LF. Although the form of this evolution is not tightly constrained (e.g. they are not able to decide between pure luminosity evolution, pure density evolution, or some combination), their data are compatible with pure luminosity evolution (hereafter, PLE) of the form $L_{60\,\mu m}(z) \approx (1+z)^{k_{60}}$, with $k_{60} \approx 3$. Similar evolutionary rates in the infrared LF have also been suggested by others (e.g. Lonsdale & Hacking 1989, and references therein).

Under the above simplifying assumptions, the monochromatic XRB intensity at 2 keV from IR-emitting galaxies may be estimated from

$$I_{2\,\mathrm{keV}} = \frac{c}{4\pi H_0} \int_{z=0}^{z_{\max}} \int \left[\frac{l_{2\,\mathrm{keV}}(L_{60\,\mu m})\,\phi_0(L_{60\,\mu m})}{[(1+z)^{(2-\alpha_X-ak_{60})}\sqrt{1+2q_0 z}]} \right] \times d(\log L_{60\,\mu m})\, dz, \qquad (2)$$

where, for our estimates, the integral over $\log L_{60\,\mu m}$ is taken between limits $41.5 \le \log L_{60\,\mu m} \le 45.0$, the range relevant for $z = 0$, as discussed in Section 6.1. The 60-μm LF is taken to be zero beyond $z \ge z_{\max}$. The monochromatic luminosity at 2 keV as a function of $L_{60\,\mu m}$, $l_{2\,\mathrm{keV}}(L_{60\,\mu m})$, can be derived from equation (1) above; $\alpha_X = -0.5$ is assumed in this case.

6.2.1 *No evolution*

We consider several cases in numerically integrating equation (2) over $\log L_{60\,\mu m}$. First, we assume there is no evolution of the 60-μm LF, so that $k_{60} = 0$. We use the model parameter values corresponding to solution number 17 in table 3(a) of Saunders *et al.* (1990), but with a normalization parameter (C) consistent with our present assumption of no evolution (and with corrections to $H_0 = 50$ km s^{-1} Mpc^{-1}). Our estimate of the fractional XRB contribution, $R_{2\,\mathrm{keV}}$, as a function of $z_{\max}$, due to IR-emitting galaxies for this 'no-evolution' case is shown by the solid line labelled 'no evolution' in Fig. 5.

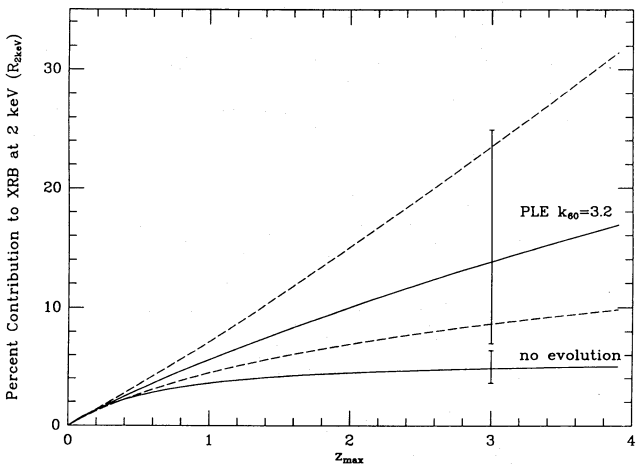

Figure 5. The percentage contribution to the XRB, $R_{2\,\mathrm{keV}}$, of IR-emitting galaxies (excluding Seyferts and QSOs) as a function of $z_{\max}$. The assumption of no evolution yields the solid curve labelled 'no evolution'. Pure luminosity evolution of the 60-μm LF with $k_{60} = 3.2$ results in the curve labelled 'PLE $k_{60} = 3.2$'. The dashed curves indicate the approximate range associated with the 1σ uncertainty in the 60-μm PLE rate k_{60} ($k_{60} = 3.2 \pm 1.0$). The error bars show the combined formal uncertainties (for $z_{\max} = 3$) in the XRB estimates, accounting for uncertainties associated with the 60-μm LF as well as the formal uncertainty in the relation between X-ray and IR luminosity (see Section 6.2).

For specific quantitative comparison, we note that the above 'no-evolution' case results in an estimate of $R_{2\,\mathrm{keV}} = 4.8^{+1.6}_{-1.2}$ per cent for integration to $z_{\max} = 3$. Our estimated 1σ error accounts for formal uncertainties in the regression parameters of equation (1) and uncertainties in the $z = 0$, 60-μm LF parameters of Saunders *et al.* In part because of our use of the Saunders *et al.* 60-μm LF, our no-evolution estimate is similar to, but lower than, values of $R_{2\,\mathrm{keV}}$ found by previous workers. For example, Weedman (1986) estimated 13 per cent, and GP about 10 per cent for the similar case of no evolution and integration in redshift to $z_{\max} = 3$. Unfortunately, the complicated selection effects present in our sample (and those used by previous workers) preclude any secure conclusion about the generality and accuracy of these results. For example, if we include Sy2 in determining best-fitting parameters for equation (1), the estimated XRB contribution of IR-emitting galaxies is higher, $R_{2\,\mathrm{keV}} = 7.6$ per cent. Such systematic uncertainties might be eliminated through X-ray studies of complete samples of IR-selected galaxies.

6.2.2 *Pure luminosity evolution*

As a second case, we now allow for pure luminosity evolution of the 60-μm LF according to $L_{60\,\mu\mathrm{m}}(z) = L_{60\,\mu\mathrm{m}}(0)\,(1+z)^{k_{60}}$. Note that k_{60} is the rate of evolution of the 60-μm LF, and so must be converted into a corresponding rate of X-ray PLE [e.g. using equation (1)], when integrating equation (2) over redshift. With such a PLE model, we now use 60-μm model LF parameters essentially the same as those of model 23 in table 3(a) of Saunders *et al.* (1990), but with small corrections for our assumed value of $q_0 = 0$, $H_0 = 50$ km s^{-1} Mpc^{-1}, functional form of the PLE, etc. Our estimate for the case of PLE with $k_{60} = 3.2$ is shown by the solid line labelled 'PLE $k_{60} = 3.2$' in Fig. 5. For this PLE model, the dashed lines in Fig. 5 show the approximate range in uncertainty of the XRB estimate due to the uncertainty in the rate of IR evolution. (Saunders *et al.* 1990 find that k_{60} is in the range 3.2 ± 1.) For such PLE cases, more substantial contributions to the soft XRB are implied. For example, to $z_{\max} = 3$, and for $k_{60} = 3.2$, we estimate an XRB contribution from IR-emitting galaxies (Sy2, Sy1, QSO excluded) of $R_{2\,\mathrm{keV}} = 14^{+11}_{-7}$ per cent. The 1σ uncertainty here additionally includes the suggested range of uncertainty in the rate of evolution of the 60-μm LF. If we include Sy2 in the regression of equation (1), the XRB estimate attains the much higher value of 30 per cent for the case of $k_{60} = 3.2$. Previous studies of the XRB contribution of IR-emitting galaxies (e.g. Weedman 1991; GP; Lonsdale & Harmon 1990) have also reached qualitatively similar conclusions for models invoking evolution.

Our conclusions are tied to our assumptions that all such galaxies have an L_X to $L_{60\,\mu\mathrm{m}}$ relationship given by equation (1). Problems associated with the use of heterogeneous and incomplete samples should eventually be overcome using data from the 'all-sky' survey being carried out by the *ROSAT* mission.

7 CONCLUSIONS

For a wide range of active and normal galaxies, we have assembled far-infrared and X-ray data from the literature and from the *IRAS* and *Einstein* databases. Although the compilation is unavoidably heterogeneous, we provide the largest, most consistent data set available for studies of the relation between emission in these two bands.

We find that galaxies with soft X-ray to infrared flux ratios greater than about 0.01 are almost certain to show broad-line optical emission. This discriminant will be valuable for finding Sy1 and QSO from comparisons of IR and X-ray surveys. A sensitive, all-sky X-ray survey like *ROSAT* is particularly well-suited to such a search in conjunction with the *IRAS* data.

A significant correlation between luminosities in the 60-μm and 0.5–4.5 keV bands is found over the full data set, with a strong offset separating broad-line (BL) from normal and narrow-line (NL) galaxies. We interpret the jump toward higher X-ray emission in BL galaxies as evidence for the increasing importance of a non-thermal nuclear source.

If, as is traditional, we assume that the intrinsic dependence in galaxies is of X-ray emission on the infrared, we find a non-linear relationship between the two variables for both the BL and the NL branches such that the ratio $L_X/L_{60\,\mu\mathrm{m}}$ *decreases* with increasing L_X. We caution that non-linear trends may be found in either direction when regressing on either one of the variables alone. The mean of regressions performed on both variables is usually consistent with a linear slope.

For all properties tested, we find a continuum between Seyfert 1 galaxies and radio-quiet quasars (RQQ), confirming that their distinction is mostly one of luminosity. When separate galaxy classes are analysed, no correlation between L_X and $L_{60\,\mu\mathrm{m}}$ exists either for Seyferts, or for RQQ. Since the ratios $L_X/L_{60\,\mu\mathrm{m}}$ differ significantly between predominantly thermal and non-thermal nuclear components, we conjecture that the correlations intrinsic to each individual component are lost when the two are strongly mixed in Seyfert galaxies or RQQ.

In contrast, radio-loud quasars (RLQ) by themselves *do* show a significant correlation of L_X to $L_{60\,\mu\mathrm{m}}$. Wilkes & Elvis (1987) found that only RQQ have the steep ($\alpha \approx -1$) X-ray slopes needed to join the X-rays to the near-infrared, suggesting an intrinsic connection via a non-thermal central source between the two bands in RQQ, but not RLQ. This appears to be contradicted by our finding that only RLQ show a strong correlation between X-rays and far-infrared luminosity.

Infrared warm galaxies (those having flatter IR spectra) tend to be more powerful X-ray emitters. The IR spectral indices $\alpha(25, 60)$ and $\alpha(60, 100)$ correlate strongly with L_X over the full data set. When restricted to BL galaxies, only the correlation with $\alpha(60, 100)$ becomes weak. This colour is a measure of the relative quantity of cool dust in the galaxy, and is expected to correlate with the strength and extent of star-forming regions, but is a poor predictor of nuclear luminosities. In concordance with these expectations, only this same correlation remains strong when restricted to NL galaxies.

Since they are much more numerous, lower luminosity X-ray emitting galaxies offer an attractive alternative to QSO as the discrete source of the cosmic diffuse X-ray background radiation, one that might account for both its observed isotropy and intensity. Our analysis of the empirical relationship between L_X and $L_{60\,\mu\mathrm{m}}$ for normal and narrow optical emission-line galaxies (but excluding Seyfert 2s)

allows us to convert published 60-μm *IRAS* luminosity functions into estimates of the 2-keV X-ray luminosity function (LF) of IR-emitting galaxies spanning luminosities $41.5 \leq \log L_{60\,\mu m} \leq 45.0$. The sample we use to parametrize the X-ray/infrared relationship includes more than four times as many galaxies and encompasses a range in 60-μm luminosity about 2.5 orders of magnitude greater than samples used in previous estimates (e.g. Griffiths & Padovani 1990). For two cases, we use the resulting X-ray LF to estimate the contribution of these IR-emitting galaxies to the XRB. First, we assume no evolution of the 60-μm LF, which yields an estimate of $R_{2\,\mathrm{keV}} = 5^{+2}_{-1}$ per cent for galaxies (Seyferts and QSO excluded) out to $z_{\max} = 3$. Next, we allow for pure luminosity evolution of the 60-μm LF of the form $L_{60\,\mu m}(z) \approx (1+z)^{k_{60}}$, with k_{60} in the range 3.2 ± 1. This results in an estimated XRB contribution of $R_{2\,\mathrm{keV}} = 14^{+11}_{-7}$ per cent, from IR-emitting galaxies to $z_{\max} = 3$.

Since *ROSAT* observes in a softer (0.2–2 keV) energy range than *Einstein*, it will be interesting to compare our results with those of *ROSAT*-selected AGN. Obscuration of soft X-rays can complicate clues to the intrinsic nature of AGN, whereas hard X-rays are little attenuated by even relatively high column densities. A statistical study of Seyferts and QSO comparing far-infrared to hard X-rays (HX) for a sample of known structure would thus be of interest, particularly in tandem with our study. If the ratio $L_{HX}/L_{60\,\mu m}$ does not change with aspect ratio while $L_X/L_{60\,\mu m}$ does, then the latter change is probably an obscuration effect. If they decrease together with aspect ratio then the X-rays may be beamed, while the IR is isotropic (presumably thermal). If they decrease together independently of aspect ratio, then they are probably beamed and in addition the axis of the central accretion disc may be independent of the overall angular momentum of the galaxy. Such tests promise to provide valuable discriminants between the large variety of AGN models invoking beaming, scattering and absorption effects.

ACKNOWLEDGMENTS

Thanks go to E. Feigelson and T. Isobe for providing most of the statistical software, to the referee for helping us distil these results, and to Bruce Margon for many constructive comments. J. Kruper, and C. M. Urry, B. Wilkes and D. Harris, provided (then) unpublished data and helpful discussions. This work has been supported by NASA Grants NAG8-590 and NAG5-1253.

REFERENCES

Anderson, S. F. & Margon, B., 1987. *Astrophys. J.*, **314,** 111.
Antonucci, R. R. J. & Miller, J. S., 1985. *Astrophys. J.*, **297,** 621.
Barcons, X. & Fabian, A. C., 1989. *Mon. Not. R. astr. Soc.*, **237,** 119.
Barvainis, R., 1990. *Astrophys. J.*, **353,** 419.
Bregman, J. N., Huggins, P. J., Glassgold, A. E. & Kinney, A. L., 1985. *Astrophys. J.*, **291,** 505.
Brown, B. W. M., Hollander, M. & Korwar, R. M., 1974. In: *Reliability and Biometry,* p. 327, eds Proschan, F. & Serfling, R. J., SIAM, Philadelphia.
Canizares, C. R., Fabbiano, G. & Trinchieri, G., 1987. *Astrophys. J.*, **312,** 503.
Dahari, O. & DeRobertis, M. M., 1988. *Astrophys. J.*, **331,** 727.
Danese, L., de Zotti, G., Franceschini, A. & Toffolatti, L., 1987. *Astrophys. J. Lett.*, **318,** L15.
Done, C., Ward, M. J., Fabian, A. C., Kunieda, H., Tsuruta, S., Lawrence, A., Smith, M. G. & Wamsteker, W., 1990. *Mon. Not. R. astr. Soc.*, **243,** 713.
Eales, S. A. & Arnaud, K. A., 1988. *Astrophys. J.*, **324,** 193.
Edelson, R. A., Malkan, M. A. & Rieke, G. H., 1987. *Astrophys. J.*, **321,** 233.
Elvis, M. & Van Speybroeck, L. P., 1982. *Astrophys. J. Lett.*, **257,** L51.
Fabbiano, G., 1989. *Ann. Rev. Astr. Astrophys.*, **27,** 87.
Fabbiano, G. & Panagia, N., 1983. *Astrophys. J.*, **266,** 568.
Fabbiano, G. & Trinchieri, G., 1984. *Astrophys. J.*, **286,** 491.
Fabbiano, G. & Trinchieri, G., 1987. *Astrophys. J.*, **315,** 46.
Fabbiano, G., Feigelson, E. & Zamorani, G., 1982. *Astrophys. J.*, **256,** 397.
Fabbiano, G., Gioia, I. M. & Trinchieri, G., 1988. *Astrophys. J.*, **324,** 749.
Fabbiano, G., Trinchieri, G. & MacDonald, A., 1984. *Astrophys. J.*, **284,** 65.
Feigelson, E. D. & Berg, C. J., 1983. *Astrophys. J.*, **269,** 400.
Feigelson, E. D. & Nelson, P. I., 1985. *Astrophys. J.*, **293,** 192.
Forman, W., Jones, C. & Tucker, W. H., 1985. *Astrophys. J.*, **293,** 102.
Forman, W., Schwarz, J., Jones, C., Liller, W. & Fabian, A. C., 1979. *Astrophys. J. Lett.*, **234,** L27.
Fosbury, R. A. E. & Sansom, A. E., 1983. *Mon. Not. R. astr. Soc.*, **204,** 1231.
Gioia, I. *et al.*, 1990. *Astrophys. J. Suppl.*, **72,** 567.
Green, P. J., Ward, M. J., Anderson, S. F., Margon, B., De Grijp, M. H. K. & Miley, G. K., 1989. *Astrophys. J.*, **339,** 93 (Paper I).
Griffiths, R. E. & Padovani, P., 1990. *Astrophys. J.*, **360,** 483 (GP).
Hamilton, T. T. & Helfand, D. J., 1987. *Astrophys. J.*, **318,** 93 (HH).
Heckman, T. M., Armus, L. & Miley, G., 1987. *Astrophys. J.*, **93,** 276.
Hunt, L. K., 1991. *Astrophys. J.*, **370,** 511.
IRAS Catalog and Atlases: Point Source Catalog, 1985. US Government Printing Office, Washington, DC.
Isobe, T., Feigelson, E. D. & Nelson, P. I., 1986. *Astrophys. J.*, **306,** 490.
Kinney, A. L., Bregman, J. N., Huggins, P. J., Glassgold, A. E. & Cohen, R. D., 1984. *Publs astr. Soc. Pacif.*, **96,** 398.
Kollatschny, W., Biermann, P., Fricke, K. J., Huchtmeier, W. & Witzel, A., 1983. *Astr. Astrophys.*, **119,** 80.
Kriss, G. A., 1988. *Astrophys. J.*, **324,** 809.
Kriss, G. A. & Canizares, C. R., 1985. *Astrophys. J.*, **297,** 177.
Kriss, G. A., Canizares, C. R. & Ricker, G. R., 1980. *Astrophys. J.*, **242,** 492.
Kruper, J. S., Urry, C. M. & Canizares, C. R., 1990. *Astrophys. J. Suppl.*, **74,** 347.
Ku, W. H.-M., Helfand, D. J. & Lucy, L. B., 1980. *Nature,* **288,** 323.
Lawrence, A. & Elvis, M., 1982. *Astrophys. J.*, **256,** 410.
Lawrence, A., Walker, D., Rowan-Robinson, M., Leech, K. J. & Penston, M. V., 1986. *Mon. Not. R. astr. Soc.*, **219,** 687.
Lawrence, A. *et al.*, 1991. *Mon. Not. R. astr. Soc.*, **246,** 91.
Long, K. S. & Van Spreybroeck, L. P., 1983. In: *Accretion Driven X-Ray Sources,* p. 41, eds Levin, W. & van den Heuvel, E. P. J., Cambridge University Press, Cambridge.
Lonsdale, C. J. & Hacking, P. B., 1989. *Astrophys. J.*, **339,** 712.
Lonsdale, C. J. & Harmon, R., 1991. *Adv. Space Res.*, **11,** 333.
McAlary, C. W. & Rieke, G. H., 1988. *Astrophys. J.*, **331,** 1.
Maccacaro, T. & Perola, G. C., 1981. *Astrophys. J. Lett,* **246,** L11.
Malkan, M. A. & Sargent, W. L. W., 1982. *Astrophys. J.*, **254,** 22.
Margon, B., Anderson, S. F., Mateo, M., Fich, M. & Massey, P., 1988. *Astrophys. J.*, **334,** 597.
Marshall, F. J., Holt, S. S., Mushotzky, R. F. & Becker, R. H., 1983a. *Astrophys. J.*, **266,** 470.

Marshall, F. J., Holt, S. S., Mushotzky, R. F. & Becker, R. H., 1983b. *Astrophys. J. Lett.*, **269,** L31.
Neugebauer, G., Miley, G. K., Soifer, B. T. & Clegg, P. E., 1986. *Astrophys. J.*, **308,** 815.
Owen, F. N., Helfand, D. J. & Sprangler, S. R., 1981. *Astrophys. J. Lett.*, **250,** L55.
Persic, M., DeZotti, G., Danese, L., Palumbo, G. G. C., Franceschini, A., Boldt, E. A. & Marshall, F. E., 1989. *Astrophys. J. Lett.*, **344,** L125.
Petre, R., Mushotzky, R. F., Krolik, J. H. & Holt, S. S., 1984. *Astrophys. J.*, **280,** 499.
Phillips, M. M., Charles, P. A. & Baldwin, J. A., 1983. *Astrophys. J.*, **266,** 485.
Reichert, G. A., Mason, K. O., Thorstensen, J. R. & Bowyer, S., 1982. *Astrophys. J.*, **260,** 437.
Rice, W. L., Lonsdale, C. J., Soifer, B. T., Neugebauer, G., Kopan, E. L., Lloyd, L. A., De Jong, T. & Habing, H. J., 1988. *Astrophys. J. Suppl.*, **68,** 91.
Rieke, G. H., Lebofsky, M. J., Thompson, R. I., Low, F. J. & Tokunaga, A. T., 1980. *Astrophys. J.*, **238,** 24.
Sanders, D. B., Soifer, B. T., Elias, J. H., Madore, B. F., Matthews, K., Neugebauer, G. & Scoville, N. Z., 1988. *Astrophys. J.*, **325,** 74.
Sanders, D. B., Phinney, E. S., Neugebauer, G., Soifer, B. T. & Mathews, K., 1989. *Astrophys. J.*, **347,** 29.
Saunders, W., Rowan-Robinson, M., Lawrence, A., Efstathiou, G., Kaiser, N., Ellis, R. S. & Frenk, C. S., 1990. *Mon. Not. R. astr. Soc.*, **242,** 318.
Schmitt, J. H. M. M., 1985. *Astrophys. J.*, **293,** 178.
Soifer, B. T., Sanders, D. B., Madore, B. F., Neugebauer, G., Danielson, G. E., Elias, J. H., Lonsdale, C. J. & Rice, W., 1987. *Astrophys. J.*, **320,** 238.
Spignolio, L. & Malkan, M. A., 1989. *Astrophys. J.*, **342,** 83.
Steiner, J., 1981. *Astrophys. J.*, **250,** 469.
Steiner, J., Grindlay, J. & Maccacaro, T., 1982. *Astrophys. J.*, **259,** 482.
Stewart, G. C., Fabian, A. C., Terlevich, R. J. & Hazard, C., 1982. *Mon. Not. R. astr. Soc.*, **200,** 61P.
Tananbaum, H., Avni, Y., Green, R. F., Schmidt, M. & Zamorani, G., 1986. *Astrophys. J.*, **305,** 57.
Terlevich, R. & Melnick, J., 1985. *Mon. Not. R. astr. Soc.*, **213,** 841.
Trinchieri, G. & Fabbiano, G., 1985. *Astrophys. J.*, **296,** 447.
Ulvestad, J. S. & Wilson, A. S., 1983. *Astrophys. J.*, **88,** 253.
Véron-Cetty, M. P. & Véron, P., 1986. *Astr. Astrophys. Suppl.*, **66,** 335.
Véron-Cetty, M. P. & Véron, P., 1987. *A Catalogue of Quasars and Active Nuclei,* 3rd edn, European Southern Observatory Munich.
Ward, M., Elvis, M., Fabbiano, G., Carleton, N. P., Willner, S. P. & Lawrence, A., 1987. *Astrophys. J.*, **315,** 74.
Ward, M., Done, C., Fabian, A. C., Tennant, A. F. & Shafer, R. A., 1988. *Astrophys. J.*, **324,** 767.
Watson, M. G., Stanger, V. & Griffiths, R. E., 1984. *Astrophys. J.*, **286,** 144.
Weedman, D. W., 1986. In: *Star Formation in Galaxies,* NASA CP-2466, p. 351, ed. Lonsdale, Carol J., NASA CP-2466, Washington, D. C.
Weedman, D. W., 1991. In: *Massive Stars in Starbursts,* p. 317, eds Leitherer, C., Walborn, N., Heckman, T. & Norman, C., Cambridge University Press, Cambridge.
Wilkes, B. J. & Elvis, M., 1987. *Astrophys. J.*, **323,** 243.
Wilson, A. S., 1988. *Astr. Astrophys.*, **206,** 41.
Worrell, D. M., 1987. *Astrophys. J.*, **318,** 188.
Zamorani, J. P. *et al.*, 1981. *Astrophys. J.*, **245,** 357.

APPENDIX: STATISTICAL ANALYSIS

Inclusion of upper limits to all measurements is statistically conservative, since limits widen the dispersion of an observed distribution or reveal that an apparent correlation is caused by selection effects. In either case, a sample containing limits is in a sense 'more complete', since it contains more information on the intrinsic properties of the objects therein. According to Feigelson & Berg (1983), the redshift dependence of detected objects in a complete flux-limited sample is effectively removed from the luminosity relation with proper treatment of censored points. Our sample is far from complete, however, in the usual sense of including every object in a given field down to a certain limiting flux threshold in a given band, although the *IRAS* PSC comes as close to this as possible.

When dividing quantities with measured upper limits [e.g., $L_X/L(60\,\mu\mathrm{m})$, or $\alpha(25,60)$], ratios with lower limits are created. Each of the statistical methods described below allows only certain combinations of censoring (i.e. either upper or lower limits) in the data set. To compare results from different tests, we temporarily modify the data set when necessary by eliminating points that a given test cannot handle, or that will be misinterpreted. We always quote the test results from the method that incorporates the greatest number of original data, but results from other tests are used to check for consistency. These comparisons can be particularly revealing when the data set is small or suffers from heavy censoring.

Univariate statistics

For univariate analyses, we derive the variance, mean, and standard deviation of a distribution using 'survival analysis' (Feigelson & Nelson 1985). The Kaplan–Meier non-parametric maximum-likelihood estimator we use includes either lower or upper limits to the data. This method works well with any distribution having censoring independent of the values of the censored variable. This is clearly not a description of flux measurements in a flux-limited sample, wherein all the censored values are found near the sensitivity threshold of the survey. Here we emphasize flux ratios. Since thresholds for different flux bands are in general different, flux ratios do not suffer the same strongly non-random censoring.

To compare two samples (i.e. two different classes of galaxy) we test the 'null' hypothesis that two independent random samples subject to censoring (e.g., L_X for Sy1 and quasars) are randomly drawn from the same parent population. The programs for two sample tests that we use are the Gehan, or generalized Wilcoxon test, and the logrank test. The Kaplan–Meier method we employ to estimate the mean of a distribution containing limits only treats one 'direction' of limits at a time (i.e. only upper or lower bounds).

Means, medians, and two-sample test results are given in Table 2. In column (1), the tested parameters are listed. The class whose median and mean are shown is in column (2). The total number of galaxies in each class are then listed (column 3) along with the number of non-detections (column 4). Direction of these limits is indicated as 'U' for upper and 'L' for lower. For classes with mixed limits, the number of 'minority' limits deleted to permit evaluation of the distribution is given (column 5). The median of the distribution and the mean with its standard error are also listed (columns 6 and 7). The median is always well defined. If, however, the lowest (highest) point in the data set is an upper (lower) limit, the mean is not well defined, since the distribution is not

normalizable, and so the outlying censored point is redefined as a detection in our analyses. For these cases, we list the value of the limit at which the distribution is truncated (column 9).

Most classes are tested against the distribution for another class, listed under 'Versus' in the right-hand column of Table 2. The probability P that the 'null' hypothesis can be rejected using the given samples is expressed as a percentage from the Gehan and logrank tests (columns 10 and 11). If the probability P is low ($\leqslant 2$ per cent) that measurements of a given property for two samples arise from a single parent population (i.e. that the null hypothesis is rejected), we accept that the two samples are 'different' or 'distinct' in this property. If this two-sample test probability is high ($\geqslant 20$ per cent), we state that the samples are 'similar' or 'indistinguishable.' Intermediate values we take to be inconclusive.

Bivariate statistics

Methods

In testing the significance of correlations between variables containing censored data, we employ a generalization of Kendall's non-parametric rank correlation test developed by Brown, Hollander & Korwar (1974, hereafter BHK test). This method assumes no distribution for censoring and allows either type of censoring simultaneously in both axes. For data with no limits, these methods yield essentially the same results as the standard correlation-coefficient test.

We consider correlations between two variables to be significant if the probability P of their independence is less than 2.0 per cent in the BHK test. This is equivalent to a rejection of the 'null hypothesis' (that the two variables are unrelated) at the 98 per cent confidence level. If $P > 2$ per cent for any test, the correlation is considered to be weak. The upper right half of Table 3 displays the strength of correlations ('W' for weak, 'S' for strong) for the entire IR/X ensemble of galaxies between parameters listed across the top and left-hand sides. Symbols in parentheses indicate that, due to selection effects, other samples may be better suited to analysis of the variables involved. If the ensemble of all galaxies shows a strong correlation for parameters combining IR and X-ray data, results are tabulated in the lower left half of Table 3 for tests performed on broad and narrow optical emission-line galaxies, respectively. We do not consider a correlation across many classes to be significant unless it persists within at least one of the individual classes in the data set. All correlations shown in Table 3 are positive.

The results of regression analyses for correlations shown to be strong are tabulated in Table 4. We include regressions of $L_X(L_{60\,\mu m})$ individually for QSO, ELG and SPIRR, classes which are not shown separately in Table 3. Linear regressions are performed via one of two tests. A two-dimensional Kaplan–Meier (hereafter 2KM) test (Schmitt 1985) allows censoring (of a single type) in both variables. The number of bins for each axis used in 2KM tests is always at least 10, and thereafter the lesser of $N_{tot}/10$ and 20. The number of bootstrap simulations used in 2KM tests to determine errors on the fit parameters is N_{tot}^2 up to a maximum of 100. A second test, the EM algorithm (Isobe *et al.* 1986) assumes a normal distribution of the dependent variable about the regression line, and allows either type of censoring simultaneously, but only in the dependent variable. Results of the regression test that retains the greatest number of original data are given in Table 4.

If one knows *a priori* which of two variables is the dependent and which the independent, then regression analysis finds the linear parameters that best estimate the intrinsic function $y(x)$. (In our case, both y and x generally are logarithms, so the linear regression finds the best-fitting power-law relationship of the original variables.) If, as is usually the case, the intrinsic physical relationship is unknown, then it is not clear whether the physical mechanism is best represented by the regression of $y(x)$ or of $x(y)$. For the first regression listed in Table 4 we have arbitrarily chosen to have spectral index or luminosity ratios as the dependent variable. On the line marked 'mean $y(x)$', we also list the slope and intersect of the line that bisects the two fits shown above it, expressed in the coordinate system of the first fit. The mean slope is the same in either coordinate system, although the derived intercept in general changes.

The mean slope is most often linear to within the errors (the two fitted lines provide conservative estimates of outer limits). It is not clear to us whether the mean regression represents the best estimate of the intrinsic physical relationship. In the past, the limited statistical methods available dictated that only the dependent variable might contain upper limits, so it was generally assumed that X-rays depend intrinsically on the IR. The ideal statistical treatment would be a test based on regressions perpendicular to the best-fitting line, but, to our knowledge, such methods are not yet available for censored data in more than one axis. Also, to compare our results to published work (e.g., Worrall 1987; Kriss 1988; Sanders *et al.* 1989), we must use regressions performed only in the same direction.